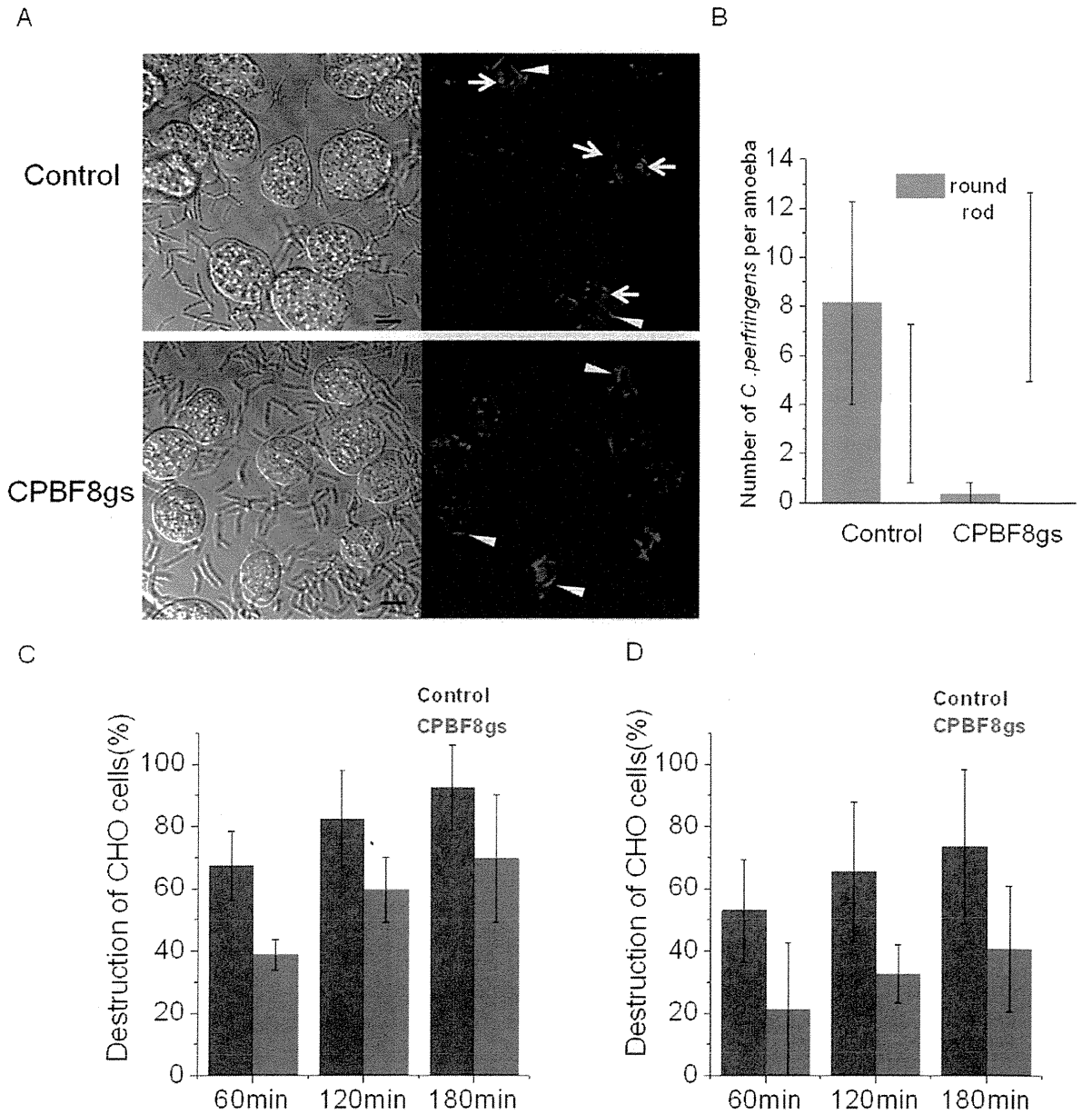

Figure 5. Effects of CPBF8 repression on the digestion of *C. perfringens* and destruction of CHO monolayers. (A) Micrographic images of control and CPBF8gs strains coincubated with *C. perfringens*. Approximately 1.5×10^4 cells of the control and CPBF8gs strains were incubated with 1.5×10^6 *C. perfringens*, pretreated with 10 μM of SYTO-59. After 4 h co-incubation, amoebas were washed and microscopically examined. Bar, 10 μm. Arrows indicate representative round shape "deformed" or "damaged" *C. perfringens*. Arrowheads indicate representative rod-shaped "intact" *C. perfringens*. (B) Quantitative analysis of rod-shaped and round *C. perfringens* in the control and CPBF8gs strains. Data shown are the means ± standard deviations of 20 independent cells. (C, D) Kinetics of CHO cell destruction by the control and CPBF8gs strains. Approximately 5×10^4 cells of the control and CPBF8gs strains, untreated (C) or pretreated with 200 μM of E-64 for 2 h and washed with PBS (D), were added to a monolayer of confluent CHO cells in 24 wells and incubated at 35°C for the indicated times. Data shown are the means ± standard deviations of four independent experiments. Monolayer destruction is expressed as the percentage of destroyed CHO cells. Data shown are the means ± standard deviations of four independent experiments.
doi:10.1371/journal.ppat.1002539.g005

mechanism may be used despite the apparent difference in the predicted strength of the membrane association (one versus 11–13 transmembrane regions, respectively). Further experiments are necessary to identify a key factor that determines cellular localization.

Cargo specificity and physiological function of CPBF8

Affinity immunoprecipitation of CPBF8 led us to identify β-hexosaminidase α-subunit and lysozymes as the major cargos of CPBF8. The cargo specificity of CPBF8 was further supported by the dramatic reduction of their enzymatic activities in both the

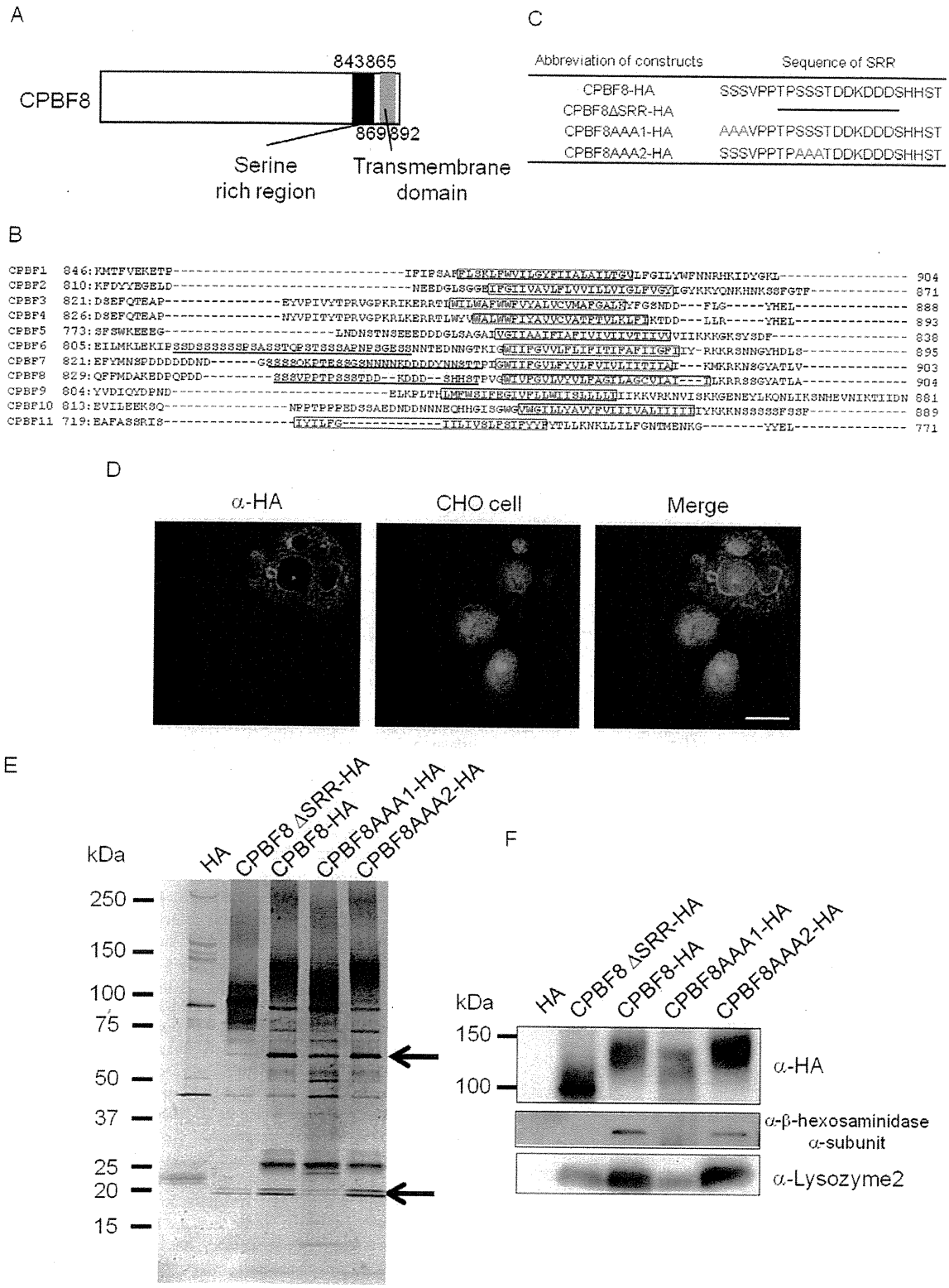

Figure 6. The serine-rich region of CPBF8 is involved in the binding with β-hexosaminidase α-subunit and lysozymes. (A) Schematic diagram of the serine-rich region and transmembrane domain in CPBF8. Numbers indicate amino acid positions from the amino terminus. The filled or hatched box depicts the serine rich region or the transmembrane domain, respectively. (B) Comparison of the carboxyl-terminal region of CPBF

proteins. Boxes indicate the putative transmembrane domain. The serine-rich region is underlined. (C) The amino acid sequences of the wild-type and mutated serine-rich regions (SRR). Note that the entire SRR was deleted in CPBF8ΔSRR-HA. The first or second stretch of three serine residues within SRR were substituted with alanines in CPBF8AAA1-HA and CPBF8AAA2-HA, respectively. (D) Localization of CPBF8ΔSRR-HA to phagosomes. Amoebae were incubated with Cell Tracker Blue-stained CHO cells (*blue*) for 60 min, fixed, and reacted with anti-HA antibody (*green*). Bar, 10 μm. (E–F) Isolation and identification of binding proteins of CPBF8-HA, CPBF8ΔSRR-HA, CPBF8AAA1-HA, and CPBF8AAA2-HA. Lysates of CPBF8-HA, CPBF8ΔSRR-HA, CPBF8AAA1-HA, and CPBF8AAA2-HA transformants were mixed with anti-HA-antibody-conjugated agarose, washed, and eluted with HA peptide. Immunoprecipitated samples were separated on SDS-PAGE and silver stained (The upper and lower arrow indicated that β-hexosaminidase α-subunit and lysozymes, respectively. (E), or blotted and reacted with anti-HA, β-hexosaminidase α-subunit and lysozyme2 antibody (F).
doi:10.1371/journal.ppat.1002539.g006

whole cell and phagosomes, by repression of *CPBF8* gene. The observation is consistent with the previous finding on the mouse fibroblast, in which knockout of a specific receptor caused decrease in the intracellular activities of β-hexosaminidase, β-galactosidase, and β-glucuronidase [47].

Although deletion or repression of hydrolase receptors often causes missecretion of cargos (e.g., [47]), repression of *CPBF8* gene did not result in missecretion of β-hexosaminidase α-subunit and lysozymes. This is also in good contrast to CPBF1, gene silencing of which caused missecretion of CP5 (Nakada-Tsukui K, et al., unpublished data). The outcome of deletion or repression of a hydrolase receptor largely varies. These data suggest that the trafficking, processing, activation, secretion, and degradation of cysteine proteases and β-hexosaminidase α-subunit/lysozymes largely differ despite they use the transport receptors that belong to the same protein family. It is likely that non- or mis-targeted β-hexosaminidaseα-subunit and lysozymes remain inactive or are swiftly degraded by proteasomes.

Lysozymes are the well-established anti-bacterial protein, which degrades the cell wall of Gram-positive bacteria. Thus, the reduction of destruction of *C. perfringens* caused by CPBF8gs can be directly attributable to the loss of lysozymes in phagosomes. It has also been reported that β-hexosaminidase in *Drosophila melanogaster* [49] and in murine macrophages is important to repress and control the growth of *Mycobacterium marinum* [49]. Therefore, the defect in the transport of β-hexosaminidase α-subunit to phagosomes may also be responsible for the decrease in degradation of *C. perfringens* in CPBF8gs strain.

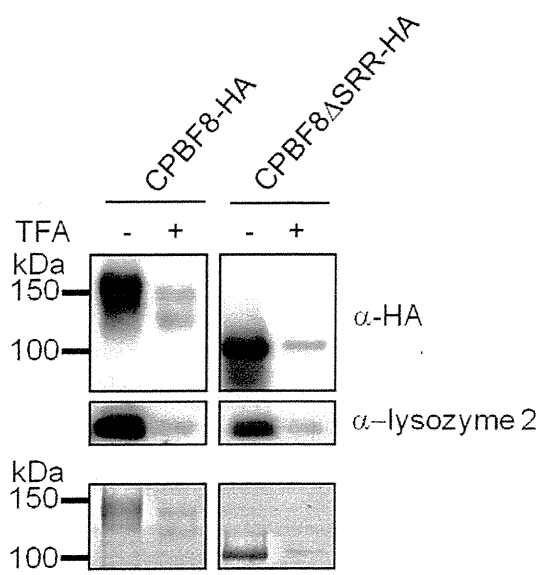

Figure 7. Post-translational modification of CPBF8. CPBF8-HA and CPBF8ΔSRR-HA was immunoprecipitated with anti-HA antibody from the lysates of CPBF8-HA and CPBF8ΔSRR-HA transformants, treated (+) or untreated (−) with TFA for 10 min. The samples were separated on SDS-PAGE and silver-stained (bottom panel), or blotted and reacted with anti-HA (top panel) or anti-lysozyme 2 antibody (middle panel). The apparent molecular weight (kDa) of standards are indicated on the left.
doi:10.1371/journal.ppat.1002539.g007

Phagosomal transport of hydrolases via CPBF8 contributes to the cytopathic activity on mammalian cells

We have shown that the cytopathic effects of trophozoites were decreased by repression of *CPBF8*, and the reduction of the cytopathy was not due to cysteine proteases, as the decrease in the cytopathy caused by *CPBF8* gene silencing was not cancelled by the cysteine protease inhibitor. These results support the premise that the enzymatic activity that decreased in CPBF8gs strain, i.e., β-hexosaminidase α-subunit and/or lysozymes, is responsible for the cytopathic effect remaining after E-64 treatment. The present study is the first to show the causal link of β-hexosaminidase α-subunit and lysozyme with virulence in eukaryotic pathogens. In mammals, β-hexosaminidase is known to hydrolyze GM2 (sphingomyelin) [6]. Recently, it has also been shown that β-hexosaminidase is involved in fertilization in hamster [50]. In addition, β-hexosaminidase from the Asian corn borer *Ostrinia furnacalis* was shown to degrade chitin [51]. Phylogenetic analysis indicated that both α and β-subunit of β-hexosaminidase from *E. histolytica* belong to the same clade as insect counterparts [52]. This clade contains two different functional β-hexosaminisases from insects. One is involved in the alteration of the structure of N-glycans generated in the cell, while the other plays in the chitin degradation processes. Although it has not been demonstrated how β-hexosaminidase is involved in the cytopathy of *E. histolytica*, it is conceivable that *E. histolytica* β-hexosaminidase degrades glycoconjugates of the extracellular matrix components to pass basement membranes, as previously suggested [53]. It was reported that lysozyme gene was poorly expressed in *E. histolytica* Rahman strain, which apparently lost virulence, and non-virulent *E. dispar*, compared to *E. histolytica* HM-1:IMSS strain [54,55]. Furthermore, lysozyme was also poorly expressed in *E. histolytica* trophozoites that were treated with 5-azacytidine (5-AzaC), a potent inhibitor of DNA methyltransferase, and showed reduced virulence [56]. Altogether, lysozymes are involved in *in vitro* cytotoxicity and *in vivo* virulence in *E. histolytica*.

The fact that CP was responsible for only 15–25% of the cytopathic effect on CHO cells in control transformant apparently disagreed to our previous finding [29], where 70–75% of the cytopathic effect in the HM-1 reference strain was attributable to CP. This is likely explained by the fact that the parental strain (G3) of the transformants for gene silencing has uncharacterized defects as well as lack of amoebapores.

Structural determinants of cargo binding in CPBF8

As mentioned above, the most striking difference between non-lysosomal/phagosomal CPBF1 and lysosomal/phagosomal CPBF8, at the primary sequence level is the serine-rich domain in

the luminal region, found exclusively in CPBF6, 7, and 8. While either the deletion of this region or point mutations of the serine stretch of the serine-rich region did not affect trafficking to phagosomes, the binding of CPBF8 to β-hexosaminidase α-subunit and lysozymes was significantly reduced. Although we cannot exclude the possibility that truncated CPBF8 was partially misfolded and thus unable to bind to its cargos, characterization of the post-translational modifications of CPBF8 via the serine-rich region by chemical removal of its potential *O*-phosphodiester-linked glycans strongly indicates that the O- phosphodiester-linked glycan within this region appears to be involved in cargo binding.

In summary, we have discovered and characterized the novel membrane-associated receptor for β-hexosaminidase α-subunit and lysozymes, CPBF8, from *E. histolytica*. We have demonstrated that CPBF8 plays an important role in the degradation of ingested bacteria in phagosomes and the cysteine protease-independent cytopathy on mammalian cells.

Materials and Methods

Microorganisms and cultivation

Trophozoites of *E. histolytica* strain HM-1:IMSS Cl-6 and G3 [41] were cultured axenically at 35°C in 13×100 mm screw-capped Pyrex glass tubes or plastic culture flasks in BI-S-33 medium as previously described [57,58]. CHO cells were grown in F-12 medium (Invitrogen, Grand Island, NY) supplemented with 10% fetal bovine serum on a 10-cm-diameter tissue culture dish (IWAKI, Tokyo, Japan) under 5% CO2 at 37°C. *Clostridium perfringens* was kindly given by Fumiya Kawahara, Nippon Institute for Biological Science Japan.

Plasmid construction and production of *E. histolytica* transformants

The protein coding region of *CPBF8* gene was amplified by PCR from cDNA using sense and antisense oligonucleotides: 5′-GCGAGATCTATGTTGGCACTCTTCGCCATC-3′ and 5′-GCGAGATCTAGCTAAAGTAGCATATCCAGA-3′ (BglII restriction sites are underlined). The amplified PCR product was digested with BglII and ligated into BglII-digested pEhExHA [28], to produce pEhEx-CPBF8-HA. The plasmid to produce the mutant form of CPBF8 that lacks 23a.a.-long serine-rich region (pEhEx-CPBF8ΔSRR-HA) was constructed as follows. A DNA sequence was amplified by PCR from pEhEx-CPBF8-HA using sense and antisense oligonucleotides: 5′-CCAGTTGGATGG-ATTGTATTTGGTGTTCTT-3′ and 5′-GTCATCTGGTT-GTGGATCTTC TTTAGCATC-3′. The PCR product was treated with BKL kit (Takara, Shiga, Japan), and self-ligated to produce pEhEx-CPBF8ΔSRR-HA. The resulting plasmid encodes a mutant CPBF8 protein lacking 843–865 a.a.-region ("SSSVPPTPSSSTDDKDDDSHHST"). Two variant forms of CPBF8 containing point mutations, S843A, S844A, and S845A, or S851A, S852A, and S853A, respectively (designated as CPBF8AAA1-HA and CPBF8AAA2-HA), are constructed as follows. DNA fragments corresponding to the portion of the protein coding region encompassing from the amino-terminal region to the mutated amino acids of CPBF8AAA1-HA and CPBF8AAA2-HA were amplified by PCR from pEhEx-CPBF8-HA, using sense and antisense oligonucleotides: 5′-ACAAACA-CATTAACAATGTTGGCACTCTTCGCC -3′ and 5′-TGG-TACTGCAGCAGCGTCATCTGGTTGTGG -3′ (for CPBF8-AAA1-HA) and 5′-ACAAACACATTAACAATGTTGGCAC-TCTTCGCC -3′ and 5′-ATCAGTTGCAGCAGCTGGT-GTTGGTGGTAC -3′ (for CPBF8AAA2-HA), where the nucleotides corresponding to the mutated amino acids (serine to alanine) are double-underlined). DNA fragments corresponding the portion of the protein coding region encompassing the mutated amino acids of to the carboxyl-terminal region of CPBF8AAA1-HA and CPBF8AAA2-HA were amplified by PCR from pEhEx-CPBF8-HA using sense and antisense oligonucleotides: 5′- GCTGCTGCAGTACCACCAACACCATCTTC-3′ and 5′- ATCATATGGATACATAGCTAAAGTAGCAT-ATCC -3′ (for CPBF8AAA1-HA), and 5′- GCTGCTGCA-ACTGATGATAAAGATGATG -3′ and 5′- ATCATATGGA-TACATAGCTAAAGTAGCATATCC-3′ (for CPBF8AAA2-HA), where the nucleotides corresponding to the mutated amino acids (serine to alanine) are double-underlined. The two amplified fragments were mixed and ligated to BglII-digested pEhExHA using GENEART Seamless ligation kit (Invitrogen, San Diego, CA, USA), to produce pEhEx-CPBF8AAA1-HA and pEhEx-CPBF8AAA2-HA. SRR-HA, which consisted of the signal peptide, SRR, the transmembrane domain, and the cytosolic region of CPBF8, was constructed as follow. A DNA fragment corresponding to the signal peptide and additional four amino acids was amplified by PCR using sense and antisense oligonucleotides: 5′- ACAAACACATTAACAATGTTGGCACTCTT-CGCC -3′ and 5′- AGAACATGTGTACTGTCCATACG-CAAC -3′. A DNA fragment corresponding to SRR, the transmembrane domain, and cytosolic region was amplified by PCR using sense and antisense oligonucleotides: 5′- CAGTACA-CATGTTCTGATGACTCTTCTTCAGTACC -3′ and 5′- AT-CATATGGATACATAGCTAAAGTAGCATATCC-3′. The two amplified fragments were mixed and ligated to BglII-digested pEhExHA using GENEART Seamless ligation kit to produce pEhEx-SRR-HA. The transformants that expressed CPBF8-HA, CPBF8ΔSRR-HA, CPBF8AAA1-HA, CPBF8AAA2-HA, or SRR-HA were established by transfection of the wild-type HM1:IMSS Cl6 strain by liposome-mediated transfection as previously described [59].

Repression of gene expression was accomplished by gene silencing, which has recently demonstrated to be mediated by nuclear localized antisense small RNAs with 5′-polyphosphate termini [42]. Gene silencing has been seen only in G3 strain, in which amoebapore genes are repressed. Thus, whatever phenotypic changes are observed by gene silencing of additional gene of interest, need to be compared against the control G3 strain transformed by the mock gene silencing plasmid (pSAP2-Gunma). Furthermore, it should be evaluated, if possible, whether the phenotypic changes are not caused by synergistic effects with amoebapore silencing. For gene silencing of *CPBF8*, *β-hexosaminidase α-subunit*, and *lysozyme 1* genes, the 420-bp-long 5′-end of the protein coding region was amplified by PCR from cDNA using sense and antisense oligonucleotides: 5′-CGCAGGCCTATG-TTGGCACTCTTCGCCATC-3′ and 5′-GCAGAGCTCAT-TTTCTTCAACTAACTTAAC-3′ (*CPBF8*); 5′-CGCAGGCCT-ATGCCATATCCAAGCTCAG-3′ and 5′-CGCGAGCTCG-TTTGATGAAATTCTAATT-3′ (*β-hexosaminidase α-subunit*); 5′-CGCAGGCCTATGTTCGCTCTCTTTTTGTG-3′ and 5′-C-GCGAGCTCACCATGGACAATACCAATAGC-3′ (*lysozyme 1*) (StuI and SacI restriction sites are underlined). The PCR-amplified DNA fragment was digested with StuI and SacI, and ligated into StuI- and SacI-digested pSAP2-gunma [60], to produce pSAP2-CPBF8, pSAP2-HexA, and pSAP2-Lys1. The gene-silenced strains were established by the transfection of G3 strain with the corresponding plasmids as described above.

Antibodies

CPBF8 and lysozyme 2 antibodies were raised against recombinant histidine-tagged partial CPBF8 (a.a. 14–292) and

full-length lysozyme 2, respectively. The method of production and purification of recombinant proteins were described before [40]. The expression plasmids for histidine-tagged CPBF8 (a.a.14–292) and lysozyme 2 were introduced into BL21(DE3) competent cells (Invitrogen). Expression of the recombinant protein was induced with 0.1 mM isopropyl-β-thiogalactoside at 37°C for 3 h. The histidine-tagged fusion protein was purified under denaturing condition using Ni-NTA agarose (QIAGEN, Hiden, Germany), according to the manufacturer's protocol. β-hexosaminidase α-subunit antibody was raised against mixture of the peptides LQQQTGLQDFKVSL (a.a. 77–90) and GWSKSKEYSDIQKF (a.a. 348–361).

Anti-HA 11MO mouse monoclonal antibody was purchased from Berkeley Antibody (Berkeley, CA). Alexa Fluor anti-mouse and antirabbit IgG and horseradish peroxidase (HRP)-conjugated goat anti-mouse were purchased from Invitrogen.

Immunofluorescene assay

For the staining of lysosomes, amoebae were incubated in the BI-S-33 medium containing LysoTracker Red DND-99 (Invitrogen) (1:500) at 35°C for 12 h. To visualize phagosomes, CHO cells were pre-stained with 10 βM of CellTracker Blue (Invitrogen) in F-12 medium supplemented with 10% fetal bovine serum at 37°C for 3 h. Labeled CHO cells were washed with phosphate-buffered saline (PBS), and added to 8-mm wells containing *E. histolytica* trophozoites on a slide glass (8 well 8 mm standard slide glass, Thermo Scientific, Rockford, IL) and further incubated at 35°C for 10–60 minutes. After the incubation, cells were fixed with 3.7% paraformaldehyde for 10 min, and permeabilized with 0.2% saponin/PBS for 10 min at ambient temperature. The cells were then reacted with anti-HA 11MO mouse monoclonal antibody (diluted at 1:1000) and Alexa Fluor-488 antimouse secondary antibody (1:1000). The samples were examined on a Carl-Zeiss LSM510 conforcal laser-scanning microscope (Thornwood, NY). Images were further analyzed using LSM510 software. We defined CPBF8-HA- and LysoTracker-positive and negative vacuoles/vesicles as follows: 1) we measured and averaged the signal intensity (per pixel) of the whole intracellular area of a cell, and also five randomly-chosen areas outside the cell to obtain a background fluorescence level; 2) for individual vacuoles/vesicles that had continuous fluorescent signal lining the membrane, two straight lines were drawn, which make a right (90-degree) angle, and a projected fluorescence histogram was obtained for each line; 3) if the peak intensity of the point on the membrane of the vacuole/vesicle was >2 fold of the background fluorescence level, the vesicle/vacuole was defined as "signal positive". The LysoTracker-positive vacuoles/vesicle was defined similarly, except that 1) the fluorescence of not a point on the membrane, but a whole intravesicular/vacuolar area was measured and averaged; and 2) the threshold of the average peak intensity of the LysoTracker-positive area in the vacuole/vesicle is >5 fold of the background fluorescence level.

Immunoprecipitation

Approximately 3×10^6 cells of CPBF8-HA-expressing amoebae were lysed in 2 ml of lysis buffer [50 mM Tris-HCl, pH 7.5, 150 mM NaCl, 1% Triton X-100 (Tokyo Kasei, Tokyo, Japan), 0.5 mg/ml E-64 (Sigma-Aldrich, St. Louis, MO)], and suitable amount of Complete mini mix (Roche, Barsel, Switzerland), and was incubated with protein G-Sepharose beads (50 µl of a 80% slurry) (Amersham Biosciences, Uppsala, Sweden) at 4°C for 90 min, centrifuged at 800× g at 4°C for 3 min to remove proteins that bind to the protein G-Sepharose beads non-specifically. The precleaned lysate was mixed with 90 µl of anti-HA-conjugated agarose (50% slurry-, Sigma-Aldrich), and incubated at 4°C for 3.5 h. The agarose beads were collected by centrifugation at 800× g at 4°C for 3 min, and washed four times using wash buffer (50 mM Tris-HCl, pH 7.5, 150 mM NaCl, 1% Triton-X 100). The agarose beads were then incubated with 180 µl of HA peptide (20 µg/ml) at 4°C for overnight to dissociate proteins from the beads. The eluate was applied to SDS-PAGE and silver staining as previously described [61].

Protein digestion, LC–MS, and MS/MS

Silver stained gels were excised, destained, and tryptic-digested using modified trypsin (Applied Biosystems Darmstadt, Germany). Briefly, excised gels were transferred to a siliconized tube, dehydrated in acetonitrile, rehydrated in 30 µl of 10 mM dithiothreitol in 0.1 M ammonium bicarbonate and reduced at room temperature for 30 min. The sample was then alkylated in 30 µl of 50 mM iodoacetamide in 0.1 M ammonomium bicarbonate at room temperature for 30 min. The reagent was removed and the sample was dehydrated in 100 µl acetonitrile, rehydrated in 100 µl of 0.1 M ammonium bicarbonate, and then dehydrated again in 100 µl acetonitrile and completely dried by vacuum centrifugation. Samples were then rehydrated in 20 ng/ml trypsin in 50 mM ammonium bicarbonate on ice for 10 min. Any excess trypsin solution was removed and 20 µl of 50 mM bicarbonate added. The samples were digested overnight at 37°C and resultant peptides were extracted in two 30 µl aliquots of 50% acetonitrile/5% formic acid. The tryptic peptides were eluted from the gel and then desalted by Ziptip. The resulting peptide mixture was separated by reverse phase chromatography (DiNa nano LC system; KYA Tech, Tokyo, Japan) using a 0.15 mm×50 mm ID HiQ sul C18W3 column (KYA Tech) and elution with 0.1% formic acid/2% CH3CN (solvent A) and 0.1% formic acid/80% CH3CN (solvent B) using a program 0% solvent B for 15 min, gradient at 4%/min for 2 min, gradient at 0.86%/min for 43 min, 11%/min for 5 min, 100% solvent B for 10 min with a total flow rate of 300 nl/min. The eluting peptides were ionized by electrospray ionization and analyzed by a 3200 Q TRAP LC/MS/MS System (Applied Biosystems). Peptide MS/MS spectra were acquired in an information-dependent manner using the Analyst QS software 2.0 acquisition features (Smart Exit, rolling collision energy, and dynamic exclusion).

Database search

Peptide sequence data obtained by mass spectrometry were analyzed against the *E. histolytica* genome database at The Institute for Genomic Research (TIGR) (http://www.tigr.org/tdb/e2k1/eha1/) using the Sequest algorithm. Sequencing data were also analyzed against the non-redundant database at the National Center of Biotechnology Information (NCBI). Individual predicted protein sequences were manually analyzed by BLAST search (http://www.ncbi.nlm.nih.gov/BLAST/) against the non-redundant database at NCBI. The identification of the protein was considered significant when at least two non-overlapping peptides of a protein were detected with the probability score >95%. The identified proteins were classified using the annotations provided in the TIGR and NCBI database and results of BLAST search.

RT-PCR

Total RNA was extracted using TRIzol reagent (Invitrogen) according to the manufacturer's instructions. The synthesis of cDNA was performed using the SuperScript III First Strand Synthesis System (Invitrogen) according to the manufacturer's instructions. The cDNA synthesis was completed on a DNA Engine Peltier Thermal Cycle (Bio-Rad Laboratories, Inc.,

Hercules, CA, USA) and treated with deoxyribonuclease I (Invitrogen) to exclude genomic DNA. PCR was performed with the resulting cDNA as a template and specific oligonucleotide primers. Primers used were 5′ (-CAAGTGCTTCAAGTACTCAACCATC-3′and 5′-ACCATTGTTACTTCTCTTTTTACGA-3′ (*CPBF6*); 5′-ATTTTATATGAACTCTCCAGACGAT-3′ and 5′-TAATAGTAATAATCAGCACAATAAC-3′ (*CPBF7*). 5′-AGAAGGTTTTGTCGATGTTCAATTC-3′ and 5′-TAACACATCCAGCAAGAATACCAGC-3′ (*CPBF8*). PCR reaction mixture contains 0.2 U of high-fidelity DNA polymerase (Phusion, FINNZYME, Espoo, Finland), 5×Phusion buffer, 0.16 mmol/L of each dNTPs, 0.5 μM Primers. Parameters for PCR were: an initial step of denaturation at 98°C for 30 sec, 25 cycles of amplification (at 98°C for 5 sec, 53°C for 20 sec, and 72°C for 2 min), and a final extension at 72°C for 5 min.

Microarray analysis

Expression analysis was performed using a custom *E. histolytica* array from Affymetrix, Inc. (Santa Clara, CA, USA), as previously described [62]. Labeled cRNA for hybridization was prepared from 5 μg of total RNA according to published Affymetrix protocol. Hybridization and scanning were performed according to Affymetrix protocols.

Preparation of cell lysates and culture supernatants

A semi-confluent culture was harvested at 48–72 h after initiation of the culture and resuspended in modified Opti-MEM (Invitrogen), Opti-MEM supplemented with 1 mg/ml ascorbic acid and 5 mg/ml cysteine. Approximately 4×10^5 amoebae in 1 ml of the medium were seeded to wells of a 12-well plate. After the culture was incubated at 35.5°C for 2 h, the culture supernatant was centrifuged at 400× g for 5 min at 4°C to remove debris. The plates were chilled on ice for 5 min and detached trophozoites were collected.

Phagosome purification

Approximately $3–5\times10^6$ trophozoites (per flask) were cultured in 25-cm^2 flasks for 48 h, and washed gently with warm modified Opti-MEM. Approximately 10^7 carboxylate-modified latex beads (Polyscience, Warrington, PA) were added to the flasks, and the flasks were centrifuged at 190× *g* for 5 min to bring the beads into contact with the trophozoites. After centrifugation, the flasks were placed on ice for 10 min. The trophozoites were washed three times with cold PBS containing 20% sucrose, followed by centrifugation at 190× *g* for 5 min to remove uningested beads. The cells containing latex beads were then resuspended in warm BI-S-33 medium, further incubated at 37°C, and harvested after 120 min. Bead-containing phagosomes were purified as previously described [12] with some modifications. Briefly, after harvesting, the amoebae that contained latex beads were resuspended in cold homogenization buffer (250 mM sucrose, pH 7.4, 3 mM imidazole, 10 mM cysteine protease inhibitor E-64, CompleteMini protease inhibitor cocktail) and homogenized with a Dounce homogenizer on ice. Phagosomes containing latex beads were then separated by flotation on a sucrose step gradient as described [12]. All sucrose solutions were made in 3 mM imidazole, pH 7.4 containing 10 mM cysteine protease inhibitor E-64. Sucrose was added to the homogenized lysate to 40%. 2 ml of the lysate containing 40% sucrose, 2 ml each of 35, 25 and 10% sucrose solutions were carefully overlaid in a 10 ml ultracentrifuge tube. The sample was centrifuged in a swinging bucket rotor MLS-50 (Beckman, Brea, CA) at 131,000× *g* at 4°C for 1 h. The phagosome fraction was collected from the interface of the 10 and 25% sucrose solutions. The collected fraction (1 ml) was mixed with 3 ml of 50% sucrose, and transferred to a new tube. To the sample, 4 ml of 25% and 2 ml of 10% sucrose solutions were overlaid, and the sample was centrifuged at 131,000× *g* at 4°C for 1 h. The separated phagosome sample, collected from the interface of the 10 and 25% sucrose solutions, was finally mixed with the same volume of 3 mM imidazole solution and centrifuged at 13,000× *g* at 4°C for 5 min. The pellet were suspended with 7% sucrose solution and stocked in −80°C.

Enzymatic assay

β-hexosaminidase assay was performed as previously described [43] with some modifications. Briefly, the reaction mixture consisted of 25 mM citrate buffer, pH 4.0, 10 mM 4-methylumbelliferyl-6-sulfo-2-acetamido-2-deoxy-β-D-glucopyranoside (MUGS)(Merck, Darmstadt, Germany) or 4-methylumbelliferyl -2-acetamido-2-deoxy-β-D-glucopyranoside (MUG)(Sigma) as substrates, and amoeba cell lysates, culture supernatant or phagosome fraction. The reaction was initiated by addition of the substrates and stopped by addition of 0.2 M glycine/0.2 M sodium carbonate, pH 10.5). The fluorescence of the released 4-methylumbelliferone was measured at excitation and emission wavelengths of 360 and 440 nm, respectively. The lysozyme assay was performed by EnzChek Lysozyme Assay Kit (Invitrogen). Briefly, the reaction mixture contained amoeba lysates, culture supernatant or phagosomal fraction and 200 μg/ml of Bodipy-conjugated *Micrococcus lysodeikticus* cell wall, and the fluorescence was measured at excitation and emission wavelengths of 485 and 530 nm, respectively. The amylase assay was performed by EnzChek amylase Assay Kit (Invitrogen). Briefly, the reaction mixture contained amoeba lysates, culture supernatant or phagosomal fraction, and 200 μg/ml of substrate solution, and the fluorescence was measured at excitation and emission wavelengths of 485 and 530 nm.

Digestion assay of *C. perfringens*

Approximately 1.5×10^4 trophozoites of control or CPBF8gs strain and 1.5×10^6 *C. perfringens* were incubated in 150 μl of BIS medium with 10 μM SYTO-59 (Invitrogen) on glass bottom culture dish(-Mattek, MA, USA) under anaerobic condition for 4 h. After incubation, the cell was washed with BIS and observed by microscopy under anaerobic condition on a Carl-Zeiss LSM510 conforcal laser-scanning microscope. The numbers of rod and round shape bacteria are counted. Images were further analyzed using LSM510 software.

In vitro translation

The soluble region of lysozyme 1 and 2 were expressed by TN SP6 High-Yield Wheat Germ Protein Expression System (Promega, WI, USA). The HA-tagged lysozyme 1 and 2 were amplified by PCR from cDNA using sense and antisense oligonucleotides: 5′- GGGGCGATCGCATGTATCCATATGATGTTCCAGATTATGCTAAATTAGGTATTGATGTCTCTC -3′ and 5′- GGGGTTTAAACTTATGGTTTGTAGTTATAATC -3′ (for HA-lysozyme 1) and 5′- GGGGCGATCGCATGTATCCATATGATGTTCCAGATTATGCTGTAGATGTATCTCAACC -3′ and 5′- GGGGTTTAAACTTAAAAATTAAATAAAAAGAAATGAG -3′ (for HA-lysozyme 2), where PmeI and SgfI restriction sites are underlined and the sequence corresponding to the HA-tag are double underlined, respectively. The PCR-amplified DNA fragments were digested with PmeI and SgfI, and ligated into PmeI- and SgfI-digested pF3A WG (BYDV) Flexi vector, to produce pF3A-HA-lysozyme 1 and 2. Expression of HA-lysozyme 1 and 2 was performed according to the manufacturer's protocol. The reactions were done at 25°C for 2 h. The purification of HA-lysozyme 1 and 2 was performed as described above for immunoprecipitation.

Cytopathic activity

CHO monolayer destruction was measured as described previously with minor modifications [63]. Briefly, CHO cells were grown with confluent in 24 well plate for over-night.at 37°C and 5% CO_2.The medium was removed and the plates were washed with modified Opti-MEM medium. Approximately 5×10^4 trophozoites of control or CPBF8gs strains were resuspended in 0.5 ml of modified Opti-MEM medium and added to each well. The plates were incubated under anaerobic conditions at 35.5°C for up to 3 h. The plates were placed on ice for 10 min to detach trophozoites. The number of CHO cells remaining in the wells was measured by WST-1 reagent (Roche) as described previously [64]. The cytopathic activity of recombinant HA-lysozyme 1 and 2 toward mammalian cells was evaluated by incubating confluent CHO cells with the mixture of purified recombinant proteins and 10% FBS/F-12 (1:99) on a 24 well plate. The plates were incubated at 35.5°C for 24 h. The number of CHO cells remaining in the wells was estimated by WST-1 reagent.

Accession numbers

CPBF1, EHI_164800, XP_655218; CPBF2, EHI_087660, XP_653276; CPBF3, EHI_161650, XP_649180; CPBF4, EHI_012340, XP_655897; CPBF5, EHI_137940, XP_654065; CPBF6, EHI_178470, XP_653036; CPBF7, EHI_040440, XP_649361; CPBF8, EHI_059830, XP_652899; CPBF9, EHI_021220, XP_655360; CPBF10, EHI_191730, XP_649015; CPBF11, EHI_118120, XP_656044; β-hexosaminidase α-subunit, EHI_148130, XP_657529; Lysozyme 1, EHI_199110, XP_653294; Lysozyme 2, EHI_096570, XP_656933

Supporting Information

Figure S1 Growth kinetics of control and CPBF8gs strains. Approximately five thousands amoebae were inoculated to 6-ml culture medium. The amoebae of each strain were counted every 24 hours. Data shown are the means ± standard deviations of five biological replicates.
(TIF)

Figure S2 Confirmation of gene silencing in β-hexosaminidase α-subunit (HexAgs) and lysozyme 1 (Lys1gs) gene-silenced strains and their ability for the destruction of CHO monolayers. (A) Reverse transcriptase-PCR analysis. A 420-bp long partial *HexA*, *Lys1*, and *Lys2* genes were amplified using cDNA from control, HexAgs, and Lys1gs strains. Abbreviations are: HexA, β-hexosaminidase α-subunit; Lys1, lysozyme 1; gs, gene-silenced. (B) The kinetics of CHO cell destruction by control, HexAgs, and Lys1gs strains. Approximately 5×10^4 cells of the control and HexAgs and Lys1gs strains were added to a monolayer of confluent CHO cells in a well of a 24-well plate and incubated at 35°C for the indicated times. Monolayer destruction is expressed as the percentage of destroyed CHO cells.
(TIF)

Figure S3 Localization of CPBF8AAA1-HA, CPBF8AAA2-HA, and SRR-HA to phagosomes. Trophozoites of CPBF8AAA1-HA (A), CPBF8AAA2-HA (B), and SRR-HA (C) were incubated with CellTracker Blue-stained CHO cells (*blue*) for 60 min, fixed, and reacted with anti-HA antibody (*green*). Bar, 10 μm.
(TIF)

Table S1 The list of all detected peptides from excised bands by LC-MS/MS.
(XLSX)

Acknowledgments

We thank Fumiya Kawahara, Nippon Institute for Biological Science, for providing *C. perfringens*. We are grateful to Yumiko Saito-Nakano, Kisaburo Nagamune, Takashi Makiuchi, and Fumika Mi-ichi for helpful discussions. The *E. histolytica* genome databases available at TIGR and Sanger, which were supported by grants from National Institute of Allergy and Infectious Diseases and Welcome Trust, were utilized for MS analysis.

Author Contributions

Conceived and designed the experiments: AF KN-T TN. Performed the experiments: AF KN-T. Analyzed the data: AF TN. Contributed reagents/materials/analysis tools: AF KN-T TN. Wrote the paper: AF KN-T TN.

Reference

1. Chipman DM, Grisaro V, Sharon N (1967) The binding of oligosaccharides containing N-acetylglucosamine and N-acetylmuramic acid to lysozyme. J Biol Chem 242: 4388–4394.
2. Muraki M, Morikawa M, Jigami Y, Tanaka H (1987) The roles of conserved aromatic amino-acid residues in the active site of human lysozyme: a site-specific mutagenesis study. Biochim Biophys Acta 916: 66–75.
3. Jollès P, Jollès J (1984) What's new in lysozyme research? Always a model system, today and yesterday. Mol Cell Biochem 53: 165–189.
4. Blake CCF, Koenig DF, Mair GA, North ACT, Phillips DC, et al. (1965) Structure of hen egg-white lysozyme. A three-dimensional fourier synthesis at 2 angstrom resolution. Nature 206: 757–761.
5. Lemansky P, Hasilik A (2001) Chondroitin sulfate is involved in lysosomal transport of lysozyme in U937 cells. J Cell Sci 114: 345–352.
6. Lemieux MJ, Mark BL, Cherney MM, Withers SG, Mahuran DJ, et al. (2006) Crystallographic structure of human beta-hexosaminidase A: interpretation of Tay-Sachs mutations and loss of GM2 ganglioside hydrolysis. J Mol Biol 359: 913–29.
7. Ozand PT, Nyhan WL, Barshop BA (2005) Part Thirteen Lipid Storage Disorders: Tay-Sachs disease/hexosaminidase A deficiency Atlas of metabolic diseases. London: Hodder Arnold. pp 539–546.
8. Gabel CA, Goldberg DE, Kornfeld S (1983) Identification and characterization of cells deficient in the mannose 6-phosphate receptor: Evidence for an alternate pathway for lysosomal enzyme targeting. Proc Natl Acad Sci U S A 80: 775–779.
9. Pohlmann R, Boeker MW, Figura FV (1995) The two mannose 6-phosphate receptors transport distinct complements of lysosomal proteins. J Biol Chem 270: 27311–27318.
10. Sonderfeld-Fresko S, Proiae R (1989) Analysis of the Glycosylation and Phosphorylation of the Lysosomal Enzyme, β-Hexosaminidase, by Site-directed Mutagenesis. J Biol Chem 264: 2692–2697.
11. Okada M, Huston CD, Mann BJ, Petri WA, Jr., Kita K, et al. (2005) Proteomic analysis of phagocytosis in the enteric protozoan parasite *Entamoeba histolytica*. Eukaryot Cell 4: 827–831.
12. Okada M, Huston CD, Oue M, Mann BJ, Petri WA, Jr., et al. (2006) Kinetics and strain variation of phagosome proteins of *Entamoeba histolytica* by proteomic analysis. Mol Biochem Parasitol 145: 171–183.
13. WHO (1997) WHO/PAHO/UNESCO report. A consultation with experts on amoebiasis. Mexico City, Mexico 28–29 January, 1997. Epidemiol Bull 18: 13–14.
14. Orozco E, Guarneros G, Martinez-Palomo A, Sanchez T (1983) *Entamoeba histolytica*: phagocytosis as a virulence factor. J Exp Med 158: 1511–21.
15. Bracha R, Mirelman D (1984) Virulence of *Entamoeba histolytica* trophozoites:effects of bacteria, microaerobic conditions, and metronidazole. J Exp Med 160: 353–68.
16. Bracha R, Kobiler D, Mirelman D (1982) Attachment and ingestion of bacteria by trophozoites of *Entamoeba histolytica*. Infect Immun 36: 396–406.
17. Tsutsumi V, Ramírez-Rosales A, Lanz-Mendoza H, Shibayama M, Chávez B, et al. (1992) *Entamoeba histolytica*: erythrophagocytosis, collagenolysis, and liver abscess production as virulence markers. Trans R Soc Trop Med Hyg 86: 170–172.
18. Guerrant RL, Brush J, Ravdin JI, Sullivan JA, Mandell GL (1981) Interaction between *Entamoeba histolytica* and human polymorphonuclear neutrophils. J Infect Dis 143: 83–93.
19. Katz U, Ankri S, Stolarsky T, Nuchamowitz Y, Mirelman D (2002) *Entamoeba histolytica* expressing a dominant negative N-truncated light subunit of its galactin are less virulent. Mol Biol Cell 13: 4256–4265.
20. Hirata KK, Que X, Melendez-Lopez SG, Debnath A, Myers S, et al. (2006) A phagocytosis mutant of *Entamoeba histolytica* is less virulent due to deficient proteinase expression and release. Exp Parasitol 115: 192–199.

21. Que X, Brinen LS, Perkins P, Herdman S, Reed SL (2002) Cysteine proteinases from distinct cellular compartments are recruited to phagocytic vesicles by *Entamoeba histolytica*. Mol Biochem Parasitol 119: 23–32.
22. Andra J, Herbst R, Leippe M (2003) Amoebapores, archaic effector peptides of protozoan origin, are discharged into phagosomes and kill bacteria by permeabilizing their membranes. Dev Comp Immunol 27: 291–304.
23. Mann BJ (2002) *Structure* and function of the *Entamoeba histolytica* Gal/GalNAc lectin. Int Rev Cytol 216: 59–80.
24. Petri WA, Jr., Haque R, Mann BJ (2002) The bittersweet interface of parasite and host: lectin-carbohydrate interactions *during human invasion by* the parasite *Entamoeba histolytica*. Annu Rev Microbiol 56: 39–64.
25. Voigt H, Olivo JC, Sansonetti P, Guillén N (1999) Myosin IB from Entamoeba histolytica is involved in phagocytosis of human erythrocytes. J Cell Sci 112: 1191–1201.
26. Marion S, Laurent C, Guillén N (2006) Signalization and cytoskeleton activity through myosin IB during the early steps of phagocytosis in Entamoeba histolytica: a proteomic approach. Cell Microbiol 7: 1504–1518.
27. Saito-Nakano Y, Yasuda T, Nakada-Tsukui K, Leippe M, Nozaki T (2004) Rab5-associated vacuoles play a unique role in phagocytosis of the enteric protozoan parasite Entamoeba histolytica. J Biol Chem 279: 49497–49507.
28. Saito-Nakano Y, Mitra BN, Nakada-Tsukui K, Sato D, Nozaki T (2007) Two Rab7 isotypes, EhRab7A and EhRab7B, play distinct roles in biogenesis of lysosomes and phagosomes in the enteric protozoan parasite *Entamoeba histolytica*. Cell Microbiol 9: 1796–1808.
29. Mitra BN, Saito-Nakano Y, Nakada-Tsukui K, Sato D, Nozaki T (2007) Rab11B small GTPase regulates secretion of cysteine proteases in the enteric protozoan parasite *Entamoeba histolytica*. Cell Microbiol 9: 2112–2125.
30. Buss SN, Hamano S, Vidrich A, Evans C, Zhang Y, et al. (2010) Members of the *Entamoeba histolytica* transmembrane kinase family play non-redundant roles in growth and phagocytosis. Int J Parasitol 40: 833–843.
31. Somalata, Bhattacharya S, Bhattacharya A (2011) A C2 domain protein kinase initiates phagocytosis in the protozoan parasite *Entamoeba histolytica*. Nat Commun 2: 230.
32. Boettner DR, Huston CD, Linford AS, Buss SN, Houpt E, et al. (2008) *Entamoeba histolytica* phagocytosis of human erythrocytes involves PATMK, a member of the transmembrane kinase family. PLoS Pathog 4: e8. doi:10.1371/journal.ppat.0040008.
33. Labruyere E, Zimmer C, Galy V, Olivo-Marin JC, Guillen N (2003) EhPAK, a member of the p21-activated kinase family, is involved in the control of *Entamoeba histolytica* migration and phagocytosis. J Cell Sci 116: 61–71.
34. Ghosh S, Samuelson J (1997) Involvement of p21racA, phosphoinositide 3-kinase, and vacuolar ATPase in phagocytosis in bacteria and erythrocytes by *Entamoeba histolytica*: suggestive evidence for coincidental evolution of amebic invasiveness. Infect Immun 65: 4243–4249.
35. Nakada-Tsukui K, Okada H, Mitra BN, Nozaki T (2009) Phosphatidylinositol-phosphates mediate cytoskeletal reorganization during phagocytosis via a unique modular protein consisting of RhoGEF/DH and FYVE domains in the parasitic protozoon *Entamoeba histolytica*. Cell Microbiol 11: 1471–1491.
36. Bruchhaus I, Jacobs T, Leippe M, Tannich E (1996) *Entamoeba histolytica* and *Entamoeba dispar*: Differences in numbers and expression of cysteine proteinase genes. Mol Microbiol 22: 255–263.
37. Willhoeft U, Hamann L, Tannich E (1999) A DNA sequence corresponding to the gene encoding cysteine proteinase 5 in *Entamoeba histolytica* is present and positionally conserved but highly degenerated in *Entamoeba dispar*. Infect Immun 67: 5925–5929.
38. Ankri S, Stolarsky T, Bracha R, Padilla-Vaca F, Mirelman D (1999) Antisense inhibition of expression of cysteine proteinases affects *Entamoeba histolytica*-induced formation of liver abscess in hamsters. Infect Immun 67: 421–422.
39. Jackson JB (1991) The proton-translocating nicotinamide adenine dinucleotide transhydrogenase. J Bioenerg Biomembr 23: 715–741.
40. Yousuf MA, Mi-ichi F, Nakada-Tsukui K, Nozaki T (2010) Localization and targeting of an unusual pyridine nucleotide transhydrogenase in *Entamoeba histolytica*. Eukaryot Cell 9: 926–33.
41. Bracha R, Nuchamowitz Y, Mirelman D (2003) Transcriptional silencing of an amoebapore gene in *Entamoeba histolytica*: Molecular analysis and effect on pathogenicity. Eukaryot Cell 2: 295–305.
42. Zhang H, Alramini H, Tran V, Singh U (2011) Nuclear localized antisense small RNAs with 5′-polyphosphate termini regulate long-term transcriptional gene silencing in entamoeba histolytica G3 strain. J Biol Chem 286: 44467–44479.
43. Hepbildikler ST, Sandhoff R, Kolzer M, Proia RL, Sandhoff K (2002) Physiological substrates for human lysosomal beta-hexosaminidase S. J Biol Chem 277: 2562–2572.
44. Ankri S, Stolarsky T, Mirelman D (1998) Antisense inhibition of expression of cysteine proteinases does not affect *Entamoeba histolytica* cytopathic or haemolytic activity but inhibits phagocytosis. Mol Microbiol 28: 777–785.
45. Hellberg A, Nickel R, Lotter H, Tannich E, Bruchhaus I (2001) Overexpression of cysteine proteinase 2 in *Entamoeba histolytica* or *Entamoeba dispar* increases amoeba-induced monolayer destruction in vitro but does not augment amoebic liver abscess formation in gerbils. Cell Microbiol 3: 13–20.
46. Moody-Haupt S, Patterson JH, Mirelman D, McConville MJ (2000) The major surface antigens of *Entamoeba histolytica* trophozoites are GPI-anchored proteophosphoglycans. J Mol Biol 297: 409–420.
47. Ludwig T, Munier-Lehmann H, Bauer U, Hollindhead M, Hoflack B (1994) Differential Sorting of lysosomal enzymes in mannose 6-phosphate receptor-deficient fibroblasts. EMBO J 13: 3430–3437.
48. Lefrancois S, Zeng J, Hassan AJ, Canuel M, Morales CR (2003) The lysosomal trafficking of sphingolipid activator proteins (SAPs) is mediated by sortilin. EMBO J 22: 6430–6437.
49. Koo IC, Ohol YM, Wu P, Morisaki JH, Cox JS, et al. (2008) Role for lysosomal enzyme beta-hexosaminidase in the control of mycobacteria infection. Proc Natl Acad Sci U S A 105: 710–715.
50. Zitta K, Wertheimer EV, Miranda PV (2006) Sperm N-acetylglucosaminidase is involved in primary bindding to the zona pellucida. Mol Hum Reprod 12: 557–563.
51. Liu T, Liu F, Yang Q, Yang J (2009) Expression, purification and characterization of the chitinolytic β-*N*-acetyl-D-hexosaminidase from the insect *Ostrinia furnacalis*. Protein Expr Purif 68: 99–103.
52. Intra J, Pavesi G, Horner DS (2008) Phylogenetic analyses suggest multiple changes of substrate specificity within the glycosyl hydrolase 20 family. BMC Evol Biol 8: 214–230.
53. Riekenberga S, Flockenhausa B, Vahrmanna A, Müller MCM, Leippe M, et al. (2004) The β-*N*-acetylhexosaminidase of *Entamoeba histolytica* is composed of two homologous chains and has been localized to cytoplasmic granules. Mol Biochem Parasitol 138: 217–225.
54. Davis PH, Scholze J, Stanley SL, Jr. (2007) Transcriptomic comparison of two *Entamoeba histolytica* strains with defined virulence phenotypes identifies new virulence factor candidates and key differences in the expression patterns of cysteine proteases, lectin light chains, and calmodulin. Mol Biochem Parasitol 151: 118–128.
55. MacFarlane RC, Singh U (2006) Identification of Differentially Expressed Genes in Virulent and Nonvirulent *Entamoeba* Species: Potential Implicationsfor Amebic Pathogenesis. Infect Immun 74: 340–351.
56. Ali IKM, Ehrenkaufer GM, Hackney JA, Singh U (2008) Growth of the protozoan parasite *Entamoeba histolytica* in 5-azacytidine has limited effects on parasite gene expression. BMC Genomics 8: 7.
57. Diamond LS, Mattern CF, Bartgis IL (1972) Viruses of *Entamoeba histolytica*. I. Identification of transmissible virus-like agents. J Virol 9: 326–341.
58. Diamond LS, Harlow DR, Cunnick CC (1978) A new medium for the axenic cultivation of *Entamoeba histolytica* and other *Entamoeba*. Trans R Soc Trop Med Hyg 72: 431–432.
59. Nozaki T, Asai T, Sanchez LB, Kobayashi S, Nakazawa M, et al. (1999) Characterization of the gene encoding serine acetyltransferase, a regulated enzyme of cysteine biosynthesis from the protist parasites *Entamoeba histolytica* and *Entamoeba dispar*. Regulation and possible function of the cysteine biosynthetic pathway in *Entamoeba*. J Biol Chem 274: 32445–32452.
60. Mi-ichi F, Makiuchi T, Furukawa A, Sato D, Nozaki T (2011) Sulfate activation in mitosomes plays a crucial role in the proliferation of *Entamoeba histolytica*. PLoS Negl Trop Dis 5: e1263.
61. Sambrook J, Russell DW (2001) Molecular Cloning. New York: Cold Spring Harbor Laboratory Press.
62. Gilchrist CA, Houpt E, Trapaidze N, Fei Z, Baba DJ (2006) Impact of intestinal colonization and invasion on the *Entamoeba histolytica* transcriptome. Mol Biochem Parasitol 147: 163–176.
63. Mitra BN, Kobayashi S, Saito-Nakano Y, Nozaki T (2006) *Entamoeba histolytica*: differences in phagosome acidification and degradation between attenuated and virulent strains. Exp Parasitol 114: 57–61.
64. Husain A, Jeelani G, Sato D, Nozaki T (2011) Global analysis of gene expression in response to L-Cysteine deprivation in the anaerobic protozoan parasite *Entamoeba histolytica*. BMC Genomics 31: 275–292.

International Immunology, Vol. 23, No. 3, pp. 195–202
doi:10.1093/intimm/dxq472

Aberrant IL-4 production by SOCS3-over-expressing T cells during infection with *Leishmania major* exacerbates disease manifestations

Mako Nakaya[1,2], Shinjiro Hamano[3], Miyuri Kawasumi[4], Hiroki Yoshida[2], Akihiko Yoshimura[1,5,6] and Takashi Kobayashi[1,4]

[1]Division of Molecular and Cellular Immunology, Medical Institute of Bioregulation, Kyushu University, Fukuoka 812-8582, Japan
[2]Department of Biomolecular Sciences, Faculty of Medicine, Saga University, 5-1-1 Nabeshima, Saga 849-8501, Japan
[3]Department of Parasitology, Institute of Tropical Medicine (NEKKEN) and the Global COE Program, Nagasaki University, Nagasaki 852-8523, Japan
[4]Center for Integrated Medical Research and [5]Department of Microbiology and Immunology Keio University School of Medicine, Shinanomachi, Shinjuku-ku, Tokyo 160-8582, Japan
[6]JST, CREST, Chiyoda-ku, Tokyo 102-0075, Japan

Correspondence to: T. Kobayashi; E-mail: takashik@z6.keio.jp

Received 28 April 2010, *accepted* 17 December 2010

Abstract

Suppressor of cytokine signaling (SOCS) 3 is a major negative feedback regulator of signal transducer and activator of transcription 3-activating cytokines. Studies using T-cell-specific SOCS3-deficient mice indicate that the absence of SOCS3 in T cells results in exacerbation of disease progression after infection by *Leishmania major* due to skewing of the T_h3 cell phenotype accompanied by hyper-production of IL-10 and transforming growth factor β (TGF-β). Here we show that transgenic mice over-expressing the *SOCS3* gene in T cells (Lck-SOCS3 Tg mice) are also susceptible to infection by *L. major*. Forced expression of SOCS3 in T cells did not affect the production of the anti-inflammatory cytokines IL-10 and TGF-β or that of the protective T_h1 type cytokine IFN-γ, which is required for parasite clearance. $CD4^+$ T cells isolated from infected-Lck-SOCS3 Tg mice produced much higher levels of IL-4 when they were re-stimulated with *L. major* antigen *in vitro*. Exacerbation of disease progression in Lck-SOCS3 Tg mice was completely reversed by administration of a neutralizing antibody against IL-4. These data suggest that tight regulation of SOCS3 expression in T_h cells is crucial for disease control during infection by *L. major*.

Keywords: regulatory T cell, T_h1, T_h2, cytokine

Introduction

The murine model of infection with the protozoan parasite *Leishmania major* has provided the first evidence of the relevance of the balance between T_h1/T_h2 cells in the regulation of disease outcome *in vivo*. Disease outcome is strongly correlated with the early patterns of T_h subset differentiation such as the IL-12 driven IFN-γ-dominated T_h1 response that promotes parasite clearance, and an IL-4-driven- and IL-4-dominated-T_h2 response that causes the development of progressive lesions (1, 2). The genetic predisposition to infection by *L. major* in mice has been studied intensively. In most inbred mouse strains (including C57BL/6), preferential differentiation towards T_h1 cells upon infection by *L. major* leads to resolution of cutaneous infection via IFN-γ-mediated activation of macrophages, whereas in some strains (e.g. BALB/c) the preferential production of IL-4 and IL-10 from T_h2 cells accompanied by reduced production of IFN-γ cannot efficiently activate macrophage leishmanicidal function (3). Disease outcome can be reversed by treatment of resistant strains with anti-IL-12 or anti-IFN-γ antibody or by treatment of susceptible strains with anti-IL-4 antibody (4–6). Furthermore, recent studies on the differentiation of T_h cells regulated by cytokine signals have revealed new T_h subsets; IL-17-producing T_h17 cells driven by transforming growth factor β (TGF-β) and IL-6 (7, 8), and immunosuppressive inducible regulatory T (iTreg) cells driven by TGF-β (9). Treg cells modulate effector immune responses (10), and the balance of $T_h1/T_h2/$

T_h17/Treg is believed to be important for the direction of immune responses. Therefore, the early differentiation of T_h cells determined by the cytokine milieu is crucial for disease outcome.

In physiological as well as pathological conditions, cytokine signals are tightly regulated by many factors, including a cytoplasmic protein family termed "suppressor of cytokine signaling (SOCS)" (11). Cytokines (including ILs and IFNs) activate the Janus kinase–signal transducer and activator of transcription (JAK–STAT) pathway. This leads to the expression of various target genes including *SOCS*. Consequently, SOCS protein inhibits its JAK–STAT activity, thereby forming a negative-feedback loop. Among the eight SOCS family proteins, SOCS3 in particular inhibits IL-6/gp130-mediated activation of STAT3 (12). We have previously shown that deletion of the *SOCS3* gene in T-cell compartments results in susceptibility to *L. major* infection, and the development of progressive lesions due to preferential production of IL-10 and TGF-β by SOCS3-deficient $CD4^+$ T cells (13). Loss of SOCS3 in T_h cells leads to excessive activation of STAT3 that enhances IL-10 and TGF-β promoter activities. It has been demonstrated that IL-10 and TGF-β exert powerful deactivating effects on infected cells. For instance, production of reactive nitrogen intermediates by IFN-γ-activated macrophages is suppressed by IL-4, IL-10 and TGF-β (14). Therefore, SOCS3 in T_h cells is a crucial factor for protective immunity against *L. major* infection.

We examined the functional significance of SOCS3 expression in T_h cells for eliminating the intracellular pathogen *L. major*. Contrary to expectations, constitutive expression of SOCS3 in T_h cells in transgenic mice carrying the *SOCS3* gene driven by the Lck-Eμ-promoter (Lck-SOCS3 Tg mice) results in exacerbation of disease progression rather than reinforced protective immunity. Lck-SOCS3-Tg mice infected with *L. major* exhibited neither an increased number of Treg populations nor enhanced production of anti-inflammatory cytokines such as IL-10 and TGF-β. However, IL-4 production by $CD4^+$ T cells from infected Lck-SOCS3 Tg mice was significantly elevated, and the administration of a neutralizing antibody against IL-4 ameliorated lesions, suggesting a skewing of the immune response toward a T_h2 phenotype in Lck-SOCS3 Tg mice during the course of infection. Taken together, temporal regulation of SOCS3 expression in T_h cells is critical for disease control of *L. major* infection.

Methods

Mice

Transgenic mice carrying the Myc-tagged wild-type *SOCS3* gene driven by the Lck-Eμ-promoter (Lck-SOCS3 Tg mice) have been described (15). Lck-SOCS3 Tg mice were backcrossed on a C57BL/6 genetic background more than 12 times. Mice were kept in specific pathogen-free facilities. Experiments using mice were approved by and carried out according to the guidelines of the Animal Ethics Committee of Kyushu University (Fukuoka, Japan).

L. major infection in mice

Leishmania major (MHOM/SU/73-5-ASKH) were passaged *in vivo* and grown *in vitro* in medium 199 with 10% heat-inactivated fetal bovine serum containing 2 mM glutamine, 10 mM HEPES and gentamicin (100 μl ml^{-1}). Infection of *L. major* was carried out as described previously (13). Briefly, 1×10^7 stationary-phase promastigotes were subcutaneously injected into the right footpad of mice. To neutralize IL-4 *in vivo*, mice were intra-peritoneally injected with 2 mg of anti-IL-4 (clone: 11B11) 5 h before and 24 h after infection. Footpad swelling was monitored every 2 weeks with a vernier caliper. Parasite burdens in the footpads were quantified by homogenizing tissue in 10 ml of the complete medium 199 as described previously (13).

Cytokine assay

Four weeks after infection by *L. major*, $CD4^+$ T cells were isolated from the right popliteal lymph nodes by MACS (Miltenyi Biotec, Bergisch Gladbach, Germany) sorting using anti-CD4 antibody (clone: GK1.5) according to the manufacturer's protocol. Cells (5×10^5 per 200 μl per well) were stimulated with or without *L. major* antigens (equivalent to 5×10^5 promastigotes) in the presence of irradiated (30 Gy) T-cell-depleted splenocytes for 70 h. Culture supernatants were collected and analyzed for IL-4, IFN-γ, TGF-β1, IL-10 and immunoglobulins by ELISA. ELISA kits were purchased from companies as follows: IFN-γ, IL-4 and IL-10 (eBioscience, San Diego, CA, USA); TGF-β (Promega, Madison, WI, USA); and mouse immunoglobulin isotype (Bethyl Laboratories Incorporated, Montgomery, TX, USA); these were used according to the manufacturers' instructions.

Flow cytometric analyses

Anti-CD4-FITC, anti-CD4-allophycocyanin (APC), anti-CD8α-FITC, anti-CD25-PE, and anti-Foxp3-APC antibodies were from eBioscience, and anti-B220-PerCP-Cy5.5 antibody was from BD Bioscience (Franklin Lakes, NJ, USA). For intracellular Foxp3 staining, popliteal lymph node cells were isolated, washed and stained with anti-CD4-FITC and anti-CD25-PE antibodies for 30 min. Cells were washed and fixed in 1× Fix/Perm solution (eBioscience) for 2 h on ice. Cells were then washed and suspended in permeabilization buffer (eBioscience), stained with APC-conjugated anti-mouse Foxp3 (clone: FJK-16s), and analyzed by flow cytometry using a FACSCalibur flow cytometer (BD Bioscience). Data were analyzed using FlowJo software (Tree Star, Inc., Ashland, OR, USA).

Immunohistochemistry

Tissue samples were isolated and fixed in 10% buffered formalin and embedded in paraffin. Sections were cut, dehydrated and microwaved in 10 mM citrate buffer (pH 6.0) twice, for 5 min each time. Sections were incubated with anti-inducible nitric oxide synthase (anti-iNOS) antibody (Santa Cruz Biotechnology Inc., Santa Cruz, CA, USA; 1:100 dilution). VECTASTAIN ABC kits (Vector Laboratories, Burlingame, CA, USA) and Histofine MOUSESTAIN kit (Nichirei Biosciences, Tokyo, Japan) were used for detection. Sections were counterstained with hematoxylin. The $iNOS^+$ area was measured in five regions for each condition using ImageJ software.

Statistical analysis

The Student's paired two-tailed *t*-test was used. $P < 0.05$ was considered significant. All error bars in the figures indicate standard deviations.

Results

Exacerbation of disease progression in Lck-SOCS3 Tg mice infected with L. major

We have previously demonstrated that T-cell-specific SOCS3 deficiency leads to susceptibility to infection with *L. major* owing to preferential differentiation of immunosuppressive T_h3 cells that produce large amounts of TGF-β and IL-10. We therefore investigated whether the constitutive expression of SOCS3 in T_h cells reverses disease outcome.

Wild-type (WT) and Lck-SOCS3 Tg mice (C57BL/6 background) were subcutaneously infected with *L. major*, and lesion size was monitored (Fig. 1A and B). Footpad swelling was exacerbated significantly more in Lck-SOCS3 Tg mice than in WT mice throughout the course of infection. In Lck-SOCS3 Tg mice, lesion size remained large until 8 weeks after infection, whereas in WT mice it gradually reduced to the basal levels (Fig. 1B). We then examined the number of parasites remaining in the footpads. Four weeks after infection, the numbers of parasites in the lesions were greater in Lck-SOCS3 Tg mice than in WT mice (Fig. 1C). These results indicated that the constitutive expression of SOCS3 in T_h cells exacerbates cutaneous leishmaniasis.

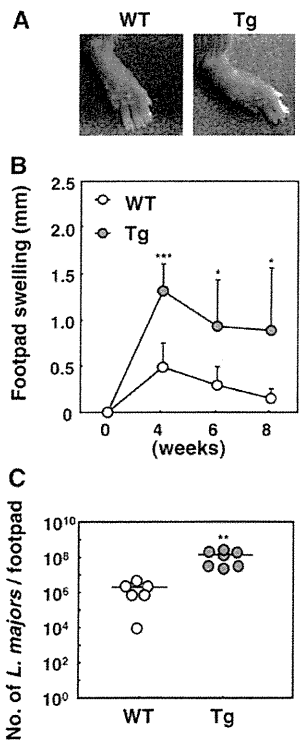

Fig. 1. Increased footpad swelling and delayed clearance of parasites in Lck-SOCS3 Tg mice. (A and B) WT and Lck-SOCS3 Tg (Tg) mice were subcutaneously infected with *Leishmania major* and photographed at 4 weeks after infection (A) and the size of footpad lesions were measured every other week (B). (C) The number of parasites in the footpad was counted 4 weeks after infection as described in Methods. Data are given as the mean ± SD ($n = 5$–7). Horizontal bars in (C) indicate the mean value in each group. ***$P < 0.001$, **$P < 0.01$, *$P < 0.05$.

The number of Treg cells does not account for exacerbation of disease progression in Lck-SOCS3 Tg mice

To reveal the molecular and cellular mechanisms underlying the progression of lesions in Lck-SOCS3 Tg mice, we initially examined the lymphocyte population in the popliteal lymph nodes. In uninfected mice, there was no significant difference in lymphocyte counts in the popliteal lymph nodes between Lck-SOCS3 Tg mice and WT mice (Fig. 2A left panel). The number of lymphocytes gradually increased after infection by *L. major*. In Lck-SOCS3 Tg mice, the lymphocyte number was slightly lower than in WT mice; this difference reached statistical significance 4 weeks after infection and became more prominent at 8 weeks after infection (Fig. 2A, right panel). The incidence of B cells among the total population of popliteal lymph node cells was greatly increased at 4 weeks after *L. major* infection, but this increase occurred in both WT and Lck-SOCS3 Tg mice to a comparable degree (WT: 75.7 ± 1.9% versus Tg: 78.9 ± 1.7%) (Fig. 2B, upper panels). In uninfected mice, a slight reduction in $CD8^+$ T cells was observed in Lck-SOCS3 Tg mice, but there was no significant difference between the two groups of mice in $CD4^+$ T-cell counts in the popliteal lymph nodes (Fig. 2C, left panel). The ratio of $CD8^+$ T cells to $CD4^+$ T cells in the T-cell compartment was significantly reduced in infected Lck-SOCS3 Tg mice (WT: 42.1 ± 1.7% versus Tg: 33.4 ± 2.0%; Fig. 2B, middle panels). Given that the total lymphocyte number in infected Lck-SOCS3 Tg mice was reduced, the cellularity of $CD8^+$ T cells was drastically reduced in Lck-SOCS3 Tg mice (Fig. 2C, right panel). The Lck promoter induces gene expression not only in peripheral T cells but also in the thymus. The phenotypes of thymocytes in uninfected mice, including percentages and actual numbers of double-negative (DN), double-positive (DP), single-positive (SP) and CD44/CD25 populations, are shown in Fig. 2(D and E). The total number of lymphocytes in the thymus was not significantly different between WT and Lck-SOCS3 Tg mice, although the numbers of CD8SP T cells were lower in Lck-SOCS3 Tg mice than in WT mice, while the numbers of $CD4^+$ T cells were comparable between the two groups (Fig. 2E). The population of DN1 was lower in Lck-SOCS3 Tg mice than in WT mice (Fig. 2D and E, lower panels). These results indicated that the reduction in $CD8^+$ T cells in Lck-SOCS3 Tg mice was an intrinsic defect of $CD8^+$ T-cell development or proliferation that occurred regardless of infection status.

Next, to analyze the frequency of Treg cells in the popliteal lymph nodes, we carried out intracellular staining for Foxp3 (a master transcription factor of Treg cells). The proportion of $CD4^+CD25^+Foxp3^+$ Treg cells in the popliteal lymph nodes of uninfected mice was identical between the two groups (WT: 10.1 ± 1.2% versus Tg: 11.1 ± 0.5%), and the frequency did not change at 4 weeks after infection (WT: 11.1 ± 1.3% versus Tg: 10.8 ± 1.5%; Fig. 2B, lower panels). This indicated that Treg cells were not involved in the exacerbated disease outcome observed in Lck-SOCS3 Tg mice.

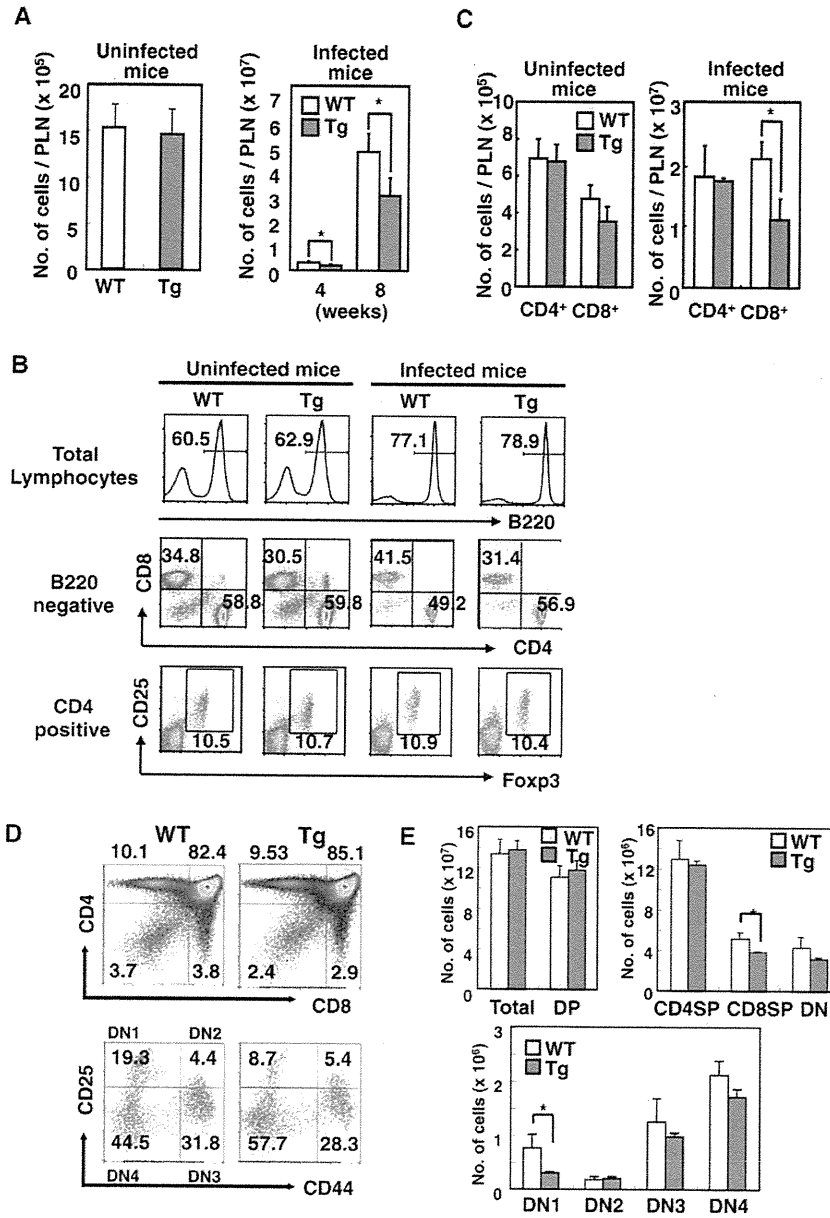

Fig. 2. Lymphocyte profiles in the draining lymph nodes of Lck-SOCS3 Tg mice infected with *Leishmania major*. (A) Cells from the popliteal lymph node were isolated from WT and Lck-SOCS3 Tg mice at 0 (uninfected), 4 and 8 weeks after infection with *L. major*, and the numbers of cells were counted (*$P < 0.05$, $n = 6$). (B) Lymph node cells were analyzed 8 weeks after infection by flow cytometry. Cells were stained for B220, CD4 and CD8 (upper and middle panels), and for CD4, CD25 and Foxp3 (lower panels). Histograms of B220 expression in the total lymph node cells and the percentages of gated B220$^-$ populations are shown in the upper panels. Profiles of CD4 versus CD8 in B220-negative populations (middle panels) and CD25 versus Foxp3 in the CD4-positive population (lower panels) are shown. The percentages of each gated area are shown. Data are representative of at least six mice for each condition. (C) The numbers of CD4$^+$ and CD8$^+$ cells in the lymph node before and 8 weeks after infection are shown (*$P < 0.05$, $n = 6$). (D) The CD4 versus CD8 profiles of total thymocytes and CD25 versus CD44 profiles of DN thymocytes in uninfected mice are shown. (E) Actual cell numbers of total, DP, CD4SP, CD8SP, DN and DN1–DN4 thymocytes are shown (*$P < 0.05$, $n = 3$).

Exacerbation of disease progression in Lck-SOCS3 Tg mice is not due to impaired production of IFN-γ or enhanced production of anti-inflammatory cytokines

We examined cytokine production by CD4$^+$ T cells derived from the popliteal lymph nodes of infected mice. IFN-γ production by CD4$^+$ T cells that were re-stimulated *in vitro* and the amount of IFN-γ in the serum were comparable between WT and Lck-SOCS3 Tg mice (Fig. 3A and B). Production of anti-inflammatory cytokines such as IL-10 and TGF-β was also comparable between the two groups of mice (Fig. 3A). These

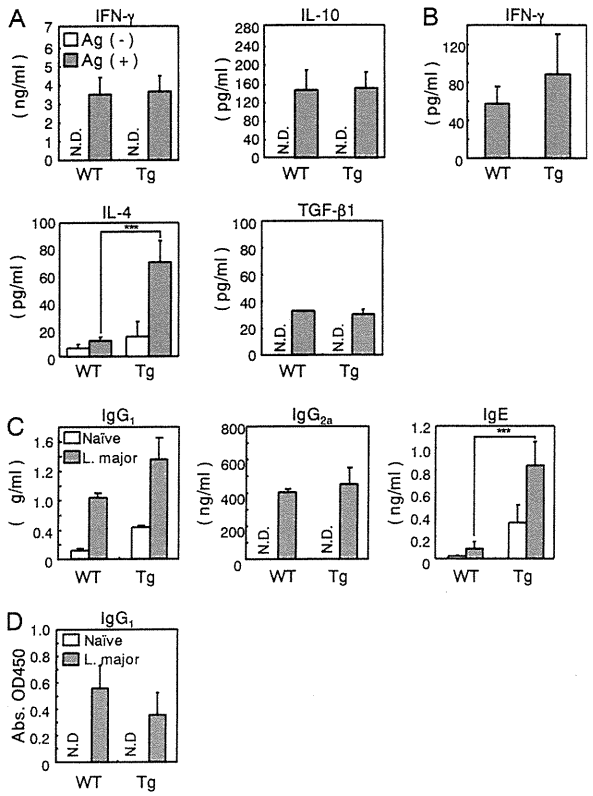

Fig. 3. Levels of cytokines and immunoglobulins in *Leishmania major*-infected Lck-SOCS3 Tg mice. (A) $CD4^+$ T cells in the popliteal lymph nodes were isolated from WT and Lck-SOCS3 Tg mice 4 weeks after infection. $CD4^+$ T cells were re-stimulated with *L. major* antigen *in vitro* in the presence of naive antigen-presenting cells for 70 h. Cytokine levels in the culture supernatant were determined by ELISA. (B) Serum IFN-γ levels at 4 weeks after infection were determined by ELISA. (C and D) Levels of total Ig (C) and *L. major* antigen-specific IgG_1 (D) in the serum from infected mice were measured by ELISA. Data are mean ± SD (n = 5–7). ***P < 0.001. ND, not detected.

results suggest that neither impaired production of IFN-γ nor enhanced production of anti-inflammatory cytokines accounts for the progression of lesions in Lck-SOCS3 Tg mice infected with *L. major*. Interestingly, IL-4 production by T cells from Lck-SOCS3 Tg mice was significantly greater than production by T cells from WT mice (Fig. 3A). Moreover, total IgG_1 and IgE levels in the serum were significantly elevated in Lck-SOCS3 Tg mice compared with levels in WT mice regardless of infection status (Fig. 3C). The levels of antigen-specific IgG_1 in the two groups of mice were comparable, however (Fig. 3D), and antigen-specific IgG_{2a} and antigen-specific IgE were below detection levels (data not shown). Thus, the increased levels of total IgG_1 and IgE may be a secondary effect of aberrant IL-4 production from T cells and may not be implicated in the exacerbation of *L. major* infection in Lck-SOCS3 Tg mice.

Neutralization of IL-4 reverses delayed clearance of parasites and increased footpad swelling in Lck-SOCS3 Tg mice

To investigate whether the enhanced production of IL-4 observed in Lck-SOCS3 Tg mice is responsible for the exacerbation of *L. major* infection, we neutralized IL-4 using a specific antibody. It is well known that neutralization of initially produced IL-4 in BALB/c mice during infection with *L. major* inhibits T_h2 cell differentiation (16). We therefore used BALB/c mice as a positive control to assess the effect of IL-4 neutralization. The increase in footpad swelling observed in Lck-SOCS3 Tg mice was completely reversed to the level seen in WT mice by administration of neutralizing antibody against IL-4 (Fig. 4A and B). The number of parasites in the lesions in Lck-SOCS3 Tg mice was also drastically reduced to the level seen in WT mice (Fig. 4C). The reduction in total lymphocytes and B cells in the popliteal lymph nodes of infected Lck-SOCS3 Tg mice was recovered by treatment with anti-IL-4 mAb (Fig. 4D and E). These results suggest that the enhanced levels of IL-4 initially produced by T_h cells in response to infection is responsible for the exacerbation of disease progression in Lck-SOCS3 Tg mice.

T_h1 effector cells produce high levels of IFN-γ, leading to the expression of iNOS and production of leishmanicidal nitric oxide in macrophages. Despite the normal level of IFN-γ production, eradication of *L. major* was dampened in Lck-SOCS3 Tg mice. We therefore compared iNOS induction in the lesions of infected mice from an immunohistochemical perspective. iNOS induction in infected tissues of Lck-SOCS3 Tg mice was much weaker than that in the tissues of WT mice, which was completely reversed by the administration of anti-IL-4 mAb (Fig. 4F and G). These results suggest that aberrant production of IL-4 by the mutant T cells suppresses iNOS induction, which is required for the elimination of intracellular pathogens.

Discussion

Cytokines and their signaling pathways define the fate and function of T_h cells, which eventually determines disease outcome. In particular, the balance between T_h1 and T_h2 cells is crucial for disease control in the *L. major* infection model (1,2). IFN-γ and IL-4 have been identified as the counter-regulatory T_h1 and T_h2 cytokines, respectively, that promote resistance and susceptibility to infection with *L. major* (4, 6, 16). The anti-inflammatory cytokines IL-10 and TGF-β, and the immunosuppressive T_h-cell subset known as Treg cells, limit the magnitude of effector responses, which contributes to the prevention of collateral damage to tissues but which may result in failure to eliminate intracellular pathogens (17–20). We have previously shown that the absence of SOCS3 in T_h cells results in exacerbation of *L. major* infection due to enhanced production of IL-10 and TGF-β caused by hyper-activation of STAT3 signaling (13).

In the present study, we examined the constitutive expression of SOCS3 in T_h cells during leishmaniasis. It has been shown that Lck-SOCS3 Tg mice show significantly enhanced airway responsiveness, suggesting that SOCS3 expression in $CD4^+$ T cells promotes T_h2-dependent responses such as allergic reaction (15). Here we found that excessive expression of SOCS3 in T cells also promoted the disease progression of leishmaniasis due to a dominant IL-4 response. Moreover, we demonstrated that aberrant IL-4 production during the early phase of infection is responsible for the exacerbation of disease progression in Lck-SOCS3 Tg mice.

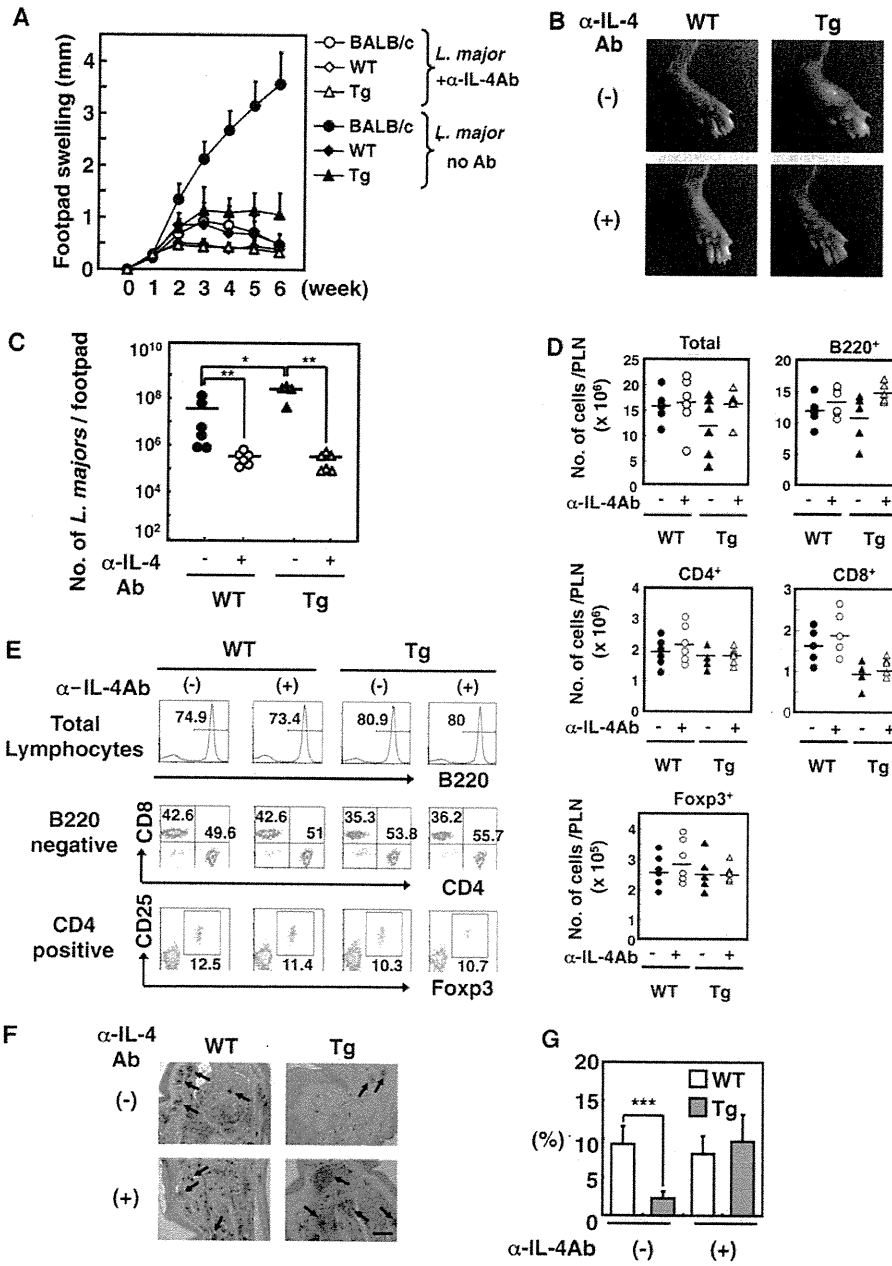

Fig. 4. Suppression of footpad swelling of *Leishmania major*-infected Lck-SOCS3 Tg mice by neutralization of initial IL-4. Mice received intraperitoneal injections of anti-mouse IL-4 antibody (α-IL-4 antibody: 2 mg per mouse) 5 h before and 24 h after infection with *L. major*. BALB/c mice were used as a positive control. (A) The size of footpad lesions was monitored weekly. (B) Photographs show lesion development in WT and Lck-SOCS3 Tg mice at 6 weeks after infection. The numbers of parasites in the footpads (C) and draining lymph node cells (D) were counted at 6 weeks after infection. (E) The lymph node cells from infected mice were analyzed by flow cytometry. (F) iNOS expression in the footpad lesions was analyzed by immunohistochemistry. Six weeks after infection, the footpad lesions were stained with anti-iNOS antibody and photographed. iNOS$^+$ areas are shown by arrows. Scale bar represents 100 μm. The iNOS$^+$ area was measured in five regions under each condition as described in Methods. Data are mean ± SD (n = 6). Horizontal bars in (C) and (D) indicate the mean value of each group. ***P < 0.001, **P < 0.01, *P < 0.05.

We found that profound expression of IL-4 was induced in Lck-SOCS3 Tg mice after infection with *L. major*. CD4$^+$ T cells from infected transgenic mice also produced a substantial amount of IFN-γ comparable with that produced by WT CD4$^+$ T cells (Fig. 3). The percentages of IFN-γ-positive T cells were comparable between the two groups of mice regardless of anti-IL-4 treatment (data not shown). Serum levels of IFN-γ in infected Lck-SOCS3 Tg mice were almost identical with those in WT mice. Moreover, the expression levels of T-bet and GATA3 in T cells were not significantly

different between the two groups of infected mice (data not shown). These results indicated that excessive production of IL-4 did not suppress the T_h1 response in Lck-SOCS3 Tg mice. Similar phenomena have been reported in which constitutive expression of IL-4 or IL-10 in resistant strains failed to control infection by *L. major* despite generating a relatively strong T_h1 response (19, 24). The mechanism by which an IFN-γ-producing T_h1 response is established under T_h2-dominated conditions *in vivo* should be resolved. Nevertheless, the T_h2 response dominates disease outcome, probably because of the deactivating effects of T_h2 cytokines on infected macrophages.

The mechanism by which IL-4 production is enhanced in T_h cells in Lck-SOCS3 Tg mice is largely unknown. It has been shown that the high expression of SOCS3 in T_h cells leads to skewing toward T_h2 differentiation, probably due in part to the inhibition of IL-12-mediated STAT4 activation by SOCS3 (15). SOCS3 binds to IL-12Rβ2 and inhibits STAT4 activation, which in turn suppresses further induction of IL-12Rβ2 expression and T_h1 development (15, 25). Selective loss of IL-12 signaling due to the down-regulation of IL-12Rβ2 expression in the susceptible BALB/c strain has also been reported (26). Defective IL-12 signaling therefore probably promotes an IL-4-dominant T_h2 response in Lck-SOCS3 Tg mice. However, the pathological relevance of the expression of IL-12Rβ2 in *L. major* infection is controversial because IL-12Rβ2 transgenic BALB/c mice are susceptible to infection by *L. major* despite normal activation of STAT4 in $CD4^+$ T cells upon IL-12 stimulation (27). Furthermore, the induction of IL-12 in response to *L. major* infection is delayed in comparison with the induction of IL-4 and IL-13, even in resistant mice (28, 29). Therefore, under pathological conditions, IL-12 may have a limited role in inhibition of the early burst of IL-4 in response to *L. major* infection.

Another possible effect of T_h2-type polarization in Lck-SOCS3 Tg mice during infection with *L. major* is impaired signaling of IL-27 (an IL-12-related cytokine induced earlier than IL-12 in response to *L. major* infection). IL-27 activates STAT1 and STAT3 through its receptor, which consists of WSX-1 and gp130 subunits, resulting in positive and negative regulations of immune responses (30). It is thought that IL-27 not only promotes T_h1 response but also suppresses IL-4 production in T_h2 cells after infection with *L. major* (25, 31). Indeed, WSX-1-deficient C57BL/6 mice are highly susceptible to *L. major* infection accompanied with increased levels of IL-4 (32). Our preliminary data indicated that activation of STAT1 and STAT3 in response to IL-27 was severely impaired in $CD4^+$ T cells from Lck-SOCS3 Tg mice (data not shown). Therefore, constitutive expression of SOCS3 in $CD4^+$ T cells may inhibit the IL-27 signal, leading to the increase in IL-4 in Lck-SOCS3 Tg mice. Further investigation is necessary to clarify the mechanism underlying the enhanced production of IL-4 in Lck-SOCS3 Tg mice.

We found that $CD8^+$ T cells were significantly reduced in infected Lck-SOCS3 Tg mice, but the number of $CD8^+$ T cells in the thymus was already decreased in uninfected mutant mice. Thus, forced expression of SOCS3 in T cells resulted in a reduction in peripheral $CD8^+$ T cells, although the mechanism behind this was uncertain. It has been reported that $CD8^+$ T cells do not play a critical role in the early phase of *L. major* infection (33). Thus, the reduction in $CD8^+$ T cells observed in Lck-SOCS3 Tg mice may not be implicated in the exacerbation of disease progression. Indeed, the reduction in $CD8^+$ T cells was not reversed by the administration of anti-IL-4 mAb, although the disease was ameliorated by the treatment.

In the present study, we revealed that SOCS3 expression in T_h cells is functionally important for eliminating *L. major*. The constitutive expression as well as the absent expression of SOCS3 in T_h cells results in exacerbation of disease progression with a different mode of action. Therefore, expression levels of SOCS3 must be regulated strictly and temporally during *L. major* infection. Taken together, the available evidence shows that temporal regulation of SOCS3 expression in T_h cells is critical for the control of *L. major* infection.

Funding

Special Grants-in-Aid for Scientific Research on Priority Areas (19041058 to T.K.), for Scientific Research on Innovative Areas (22117516 to T.K.), for Scientific Research (20590492 to T.K.), for Young Scientists (22790472 to M.N.) and Special Coordination Fund for Promoting Science and Technology Improvement of research environment for young researchers Carrier development program for young investigators in "Cell and Metabolism Research" from the Ministry of Education, Culture, Sports, Science, and Technology of Japan, the Program for Promotion of Fundamental Studies in Health Sciences of the National Institute of Biomedical Innovation (NIBIO), the Nakatomi Foundation, the Takeda Science Foundation, The Kato Memorial Trust Foundation for Nanbyo Research, the Suzuken Memorial Foundation, the Japan Intractable Disease Research Foundation, the Naito Foundation, the Mochida Memorial Foundation for Medical and Pharmaceutical Research, Astellas Foundation for Research on Metabolic Disorders, the Yakult Bioscience Research Foundation, and the Princess Takamatsu Cancer Research Fund.

Acknowledgements

We thank T. Yoshioka-Nakaji, M. Ohtsu, and N. Kinoshita for technical assistance and Y. Nishi for manuscript preparation.

References

1 Sacks, D. and Noben-Trauth, N. 2002. The immunology of susceptibility and resistance to *Leishmania major* in mice. *Nat. Rev. Immunol.* 2:845.
2 Scott, P. 1991. IFN-gamma modulates the early development of Th1 and Th2 responses in a murine model of cutaneous leishmaniasis. *J. Immunol.* 147:3149.
3 Reiner, S. L. and Locksley, R. M. 1995. The regulation of immunity to *Leishmania major*. *Annu. Rev. Immunol.* 13:151.
4 Belosevic, M., Finbloom, D. S., Van Der Meide, P. H., Slayter, M. V. and Nacy, C. A. 1989. Administration of monoclonal anti-IFN-gamma antibodies in vivo abrogates natural resistance of C3H/HeN mice to infection with *Leishmania major*. *J. Immunol.* 143:266.
5 Heinzel, F. P., Rerko, R. M., Ahmed, F. and Pearlman, E. 1995. Endogenous IL-12 is required for control of Th2 cytokine responses capable of exacerbating leishmaniasis in normally resistant mice. *J. Immunol.* 155:730.
6 Sadick, M. D., Heinzel, F. P., Holaday, B. J., Pu, R. T., Dawkins, R. S. and Locksley, R. M. 1990. Cure of murine leishmaniasis with anti-interleukin 4 monoclonal antibody. Evidence for a T cell-dependent, interferon gamma-independent mechanism. *J. Exp. Med.* 171:115.

7 Bettelli, E., Carrier, Y., Gao, W., Korn, T., Strom, T. B., Oukka, M., Weiner, H. L. and Kuchroo, V. K. 2006. Reciprocal developmental pathways for the generation of pathogenic effector TH17 and regulatory T cells. *Nature* 441:235.
8 Mangan, P. R., Harrington, L. E., O'Quinn, D. B. *et al.* 2006. Transforming growth factor-beta induces development of the Th17 lineage. *Nature* 441:231.
9 Chen, W., Jin, W., Hardegen, N. *et al.* 2003. Conversion of peripheral CD4+CD25-naive T cells to CD4+CD25+ regulatory T cells by TGF-beta induction of transcription factor Foxp3. *J Exp Med* 198:1875.
10 Xu, D., Liu, H., Komai-Koma, M. *et al.* 2003. CD4+CD25+ regulatory T cells suppress differentiation and functions of Th1 and Th2 cells, *Leishmania major* infection, and colitis in mice. *J. Immunol.* 170:394.
11 Yoshimura, A., Naka, T. and Kubo, M. 2007. SOCS proteins, cytokine signalling and immune regulation. *Nat. Rev. Immunol.* 7:454.
12 Yasukawa, H., Ohishi, M., Mori, H. *et al.* 2003. IL-6 induces an anti-inflammatory response in the absence of SOCS3 in macrophages. *Nat. Immunol.* 4:551.
13 Kinjyo, I., Inoue, H., Hamano, S. *et al.* 2006. Loss of SOCS3 in T helper cells resulted in reduced immune responses and hyperproduction of interleukin 10 and transforming growth factor-beta 1. *J. Exp. Med.* 203:1021.
14 Bogdan, C., Rollinghoff, M. and Diefenbach, A. 2000. Reactive oxygen and reactive nitrogen intermediates in innate and specific immunity. *Curr. Opin. Immunol.* 12:64.
15 Seki, Y., Inoue, H., Nagata, N. *et al.* 2003. SOCS-3 regulates onset and maintenance of Th2-mediated allergic responses. *Nat. Med.* 9:1047.
16 Chatelain, R., Varkila, K. and Coffman, R. L. 1992. IL-4 induces a Th2 response in *Leishmania major*-infected mice. *J. Immunol.* 148:1182.
17 Barral-Netto, M., Barral, A., Brownell, C. E. *et al.* 1992. Transforming growth factor-beta in leishmanial infection: a parasite escape mechanism. *Science* 257:545.
18 Belkaid, Y., Piccirillo, C. A., Mendez, S., Shevach, E. M. and Sacks, D. L. 2002. CD4+CD25+ regulatory T cells control *Leishmania major* persistence and immunity. *Nature* 420:502.
19 Groux, H., Cottrez, F., Rouleau, M. *et al.* 1999. A transgenic model to analyze the immunoregulatory role of IL-10 secreted by antigen-presenting cells. *J. Immunol.* 162:1723.
20 Powrie, F., Correa-Oliveira, R., Mauze, S. and Coffman, R. L. 1994. Regulatory interactions between CD45RBhigh and CD45RBlow CD4+ T cells are important for the balance between protective and pathogenic cell-mediated immunity. *J. Exp. Med.* 179:589.
21 Himmelrich, H., Launois, P., Maillard, I. *et al.* 2000. BALB/c mice, IL-4 production during the initial phase of infection with *Leishmania major* is necessary and sufficient to instruct Th2 cell development resulting in progressive disease. *J. Immunol.* 164:4819.
22 Julia, V., Rassoulzadegan, M. and Glaichenhaus, N. 1996. Resistance to *Leishmania major* induced by tolerance to a single antigen. *Science* 274:421.
23 Launois, P., Maillard, I., Pingel, S. *et al.* 1997. IL-4 rapidly produced by V beta 4 V alpha 8 CD4+ T cells instructs Th2 development and susceptibility to *Leishmania major* in BALB/c mice. *Immunity* 6:541.
24 Erb, K. J., Blank, C. and Moll, H. 1996. Susceptibility to *Leishmania major* in IL-4 transgenic mice is not correlated with the lack of a Th1 immune response. *Immunol. Cell Biol.* 74:239.
25 Yamamoto, K., Yamaguchi, M., Miyasaka, N. and Miura, O. 2003. SOCS-3 inhibits IL-12-induced STAT4 activation by binding through its SH2 domain to the STAT4 docking site in the IL-12 receptor beta2 subunit. *Biochem. Biophys. Res. Commun.* 310:1188.
26 Hondowicz, B. D., Park, A. Y., Elloso, M. M. and Scott, P. 2000. Maintenance of IL-12-responsive CD4+ T cells during a Th2 response in *Leishmania major*-infected mice. *Eur. J. Immunol.* 30:2007.
27 Nishikomori, R., Gurunathan, S., Nishikomori, K. and Strober, W. 2001. BALB/c mice bearing a transgenic IL-12 receptor beta 2 gene exhibit a nonhealing phenotype to *Leishmania major* infection despite intact IL-12 signaling. *J. Immunol.* 166:6776.
28 Launois, P., Swihart, K. G., Milon, G. and Louis, J. A. 1997. Early production of IL-4 in susceptible mice infected with *Leishmania major* rapidly induces IL-12 unresponsiveness. *J. Immunol.* 158:3317.
29 Reiner, S. L., Zheng, S., Wang, Z. E., Stowring, L. and Locksley, R. M. 1994. Leishmania promastigotes evade interleukin 12 (IL-12) induction by macrophages and stimulate a broad range of cytokines from CD4+ T cells during initiation of infection. *J. Exp. Med.* 179:447.
30 Hunter, C. A., Villarino, A., Artis, D. and Scott, P. 2004. The role of IL-27 in the development of T-cell responses during parasitic infections. *Immunol. Rev.* 202:106.
31 Yoshimoto, T., Yoshimoto, T., Yasuda, K., Mizuguchi, J. and Nakanishi, K. 2007. IL-27 suppresses Th2 cell development and Th2 cytokines production from polarized Th2 cells: a novel therapeutic way for Th2-mediated allergic inflammation. *J. Immunol.* 179:4415.
32 Yoshida, H., Hamano, S., Senaldi, G. *et al.* 2001. WSX-1 is required for the initiation of Th1 responses and resistance to *L. major* infection. *Immunity* 15:569.
33 Huber, M., Timms, E., Mak, T. W., Röllinghoff, M. and Lohoff, M. 1998. Effective and long-lasting immunity against the parasite *Leishmania major* in CD8-deficient mice. *Infect. Immun.* 66:3968.

特集 感染性胃腸炎の診断，治療，伝播予防

6．アメーバ赤痢やクリプトスポリジウム症の現状と最新の知見

原田 倫世* 濱野 真二郎**

生きるためには水や食物の経口的摂取が不可欠であるが，途上国など脆弱な社会基盤・衛生環境下ではしばしば病原微生物が混入し下痢を主体とした病気の原因となる。原虫は単細胞真核生物であり，細菌に対して有効な抗生物質の多くは無効である。低酸素環境である小腸や大腸に寄生するランブル鞭毛虫や赤痢アメーバにはメトロニダゾールが著効する。近年，水系集団感染の原因であり効果的な治療薬のなかったクリプトスポリジウムに対して，メトロニダゾールの類縁体であるニタゾキサニドや糸状菌から見出されたアスコフラノンが著効することが明らかとなった。本稿ではアメーバ赤痢やクリプトスポリジウム症の現状や最新の知見を概説したい。

Key Words：アメーバ赤痢／クリプトスポリジウム症／メトロニダゾール／ニタゾキサニド／アスコフラノン

I アメーバ赤痢について

アメーバ赤痢は細胞外寄生性原虫である赤痢アメーバ：*Entamoeba histolytica* によって引き起こされる感染症であり，成熟シスト（嚢子）の経口摂取によって感染する（**図1**）[1]。熱帯・亜熱帯の衛生状態の悪い地域で蔓延しており，世界中では毎年およそ4,800万人が罹患し，7万人が赤痢アメーバ感染によって死亡している。消化管症状は不顕性から下痢や粘血便を呈するものまでさまざまであり，肝臓や脳などの遠隔臓器に転移し膿瘍を形成する場合は放置すると致死的となる[2]。

わが国では2003年11月に改正された感染症法により全数把握が義務づけられた五類感染症であり，無症候性シスト排出者（キャリア）を除き，症状を有する患者を診断した医師は7日以内に最寄りの保健所に届け出る必要がある。

国立感染症研究所の感染症情報センターの発表によると，1999～2008年までの年間報告数は男女ともに毎年増加が続いており，2000年に378例であった報告数は2006年には753例，2007年には801例，2008年には861例を示したが，2009年は759例とやや減少した[3]。男女比は約8：1であり，男性が全体の85～90%を占める。同性・異性間の性的接触によるシストの経口感染も多く，本症は性行為感染症 sexually transmitted disease（**STD**）のひとつでもある。感染の推定・確定地域は国内が81%，国外が18%，不明が1%と報告されている。国外感染のアメーバ赤痢も130例（2006年）を数えるなど，旅行下痢症・輸入感染症としても注意が必要である。また，知的障害者の入居施設での集団感染も

Advances in understanding and treatment of amebiasis and cryptosporidiosis

*東京大学・大学院医学系研究科・国際保健学専攻・生物医化学教室 特任研究員 Michiyo Harada

**長崎大学・熱帯医学研究所・寄生虫学分野 教授 Shinjiro Hamano

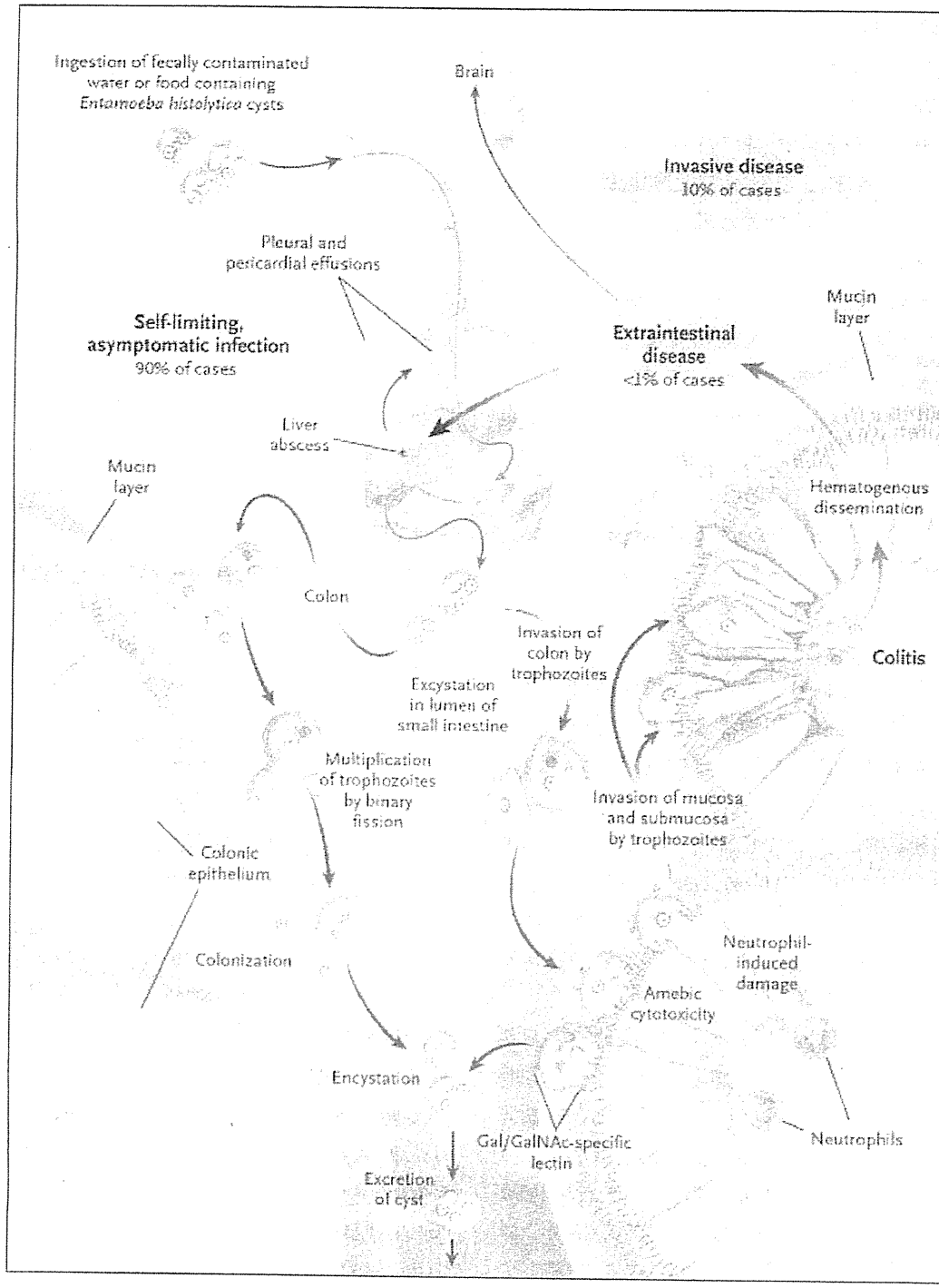

図1　赤痢アメーバの生活環

赤痢アメーバの感染は水や食物に混入した成熟シストの経口接種による。小腸管腔内で脱嚢した栄養体は大腸管腔のムチン層上で偽足を伸ばし，活発に活動・増殖する。通常，栄養体はシストを産生・排出してその生活環を完遂するため，90%の感染例は無症候性であり自然治癒する。しかしながら，ときにGal/GalNAc結合性レクチンによって介在される大腸上皮細胞への接着と傷害によって大腸への赤痢アメーバの浸潤が始まり，およそ10%の感染例は下痢や粘血便などをともなうアメーバ赤痢の病態を呈する。（文献1より）

STD (sexually transmitted disease)

報告されている。

1859年，Lamblは激しい下痢で亡くなった子どもの大腸にアメーバを見出した。これが赤痢アメーバに関する最古の記載である[4]。1875年，ロシアのLoschは木こりの大腸生検組織の中にアメーバを見出し，その患者の糞便を与えたイヌは下痢症状を呈したが，赤痢症状の原因は共存する細菌によるものであり，アメーバに病原性はないと考えた。1891年にCouncilmanとLafleurは肝膿瘍からアメーバを検出し，アメーバと疾病の因果関係を示した[5]。1903年，Schaudinnは病理学的観察にもとづき，組織“histo”を溶解“lysis”する腸内アメーバ“entamoeba”として赤痢アメーバの学名：*Entamoeba histolytica*を命名した。

赤痢アメーバは生活史上，シストと栄養体の2つの形態に区別される。赤痢アメーバの成熟シストは4核シストであり，感染者の糞便中に出現する。ヒトはこれを経口摂取することで感染する。栄養体は大腸潰瘍あるいは肝膿瘍などの病変部に検出される形態で，偽足を出して活発に活動する。下痢便の中に主として検出されるのもこの栄養体である。病原性*E. histolytica*はシスト・栄養体ともにヒト寄生性で，かつ非病原性アメーバである*E. dispar*や*E. moshkovskii*と形態学的に区別できない。

1980年代に，進んだ分子生物学的技術の進展・普及により，病原性*E. histolytica*と非病原性*E. dispar*がアイソザイムパターンやDNA解析により明確に区別されるようになった。この概念がはっきり示されたのは1993年であり[6]，WHOが正式に認定したのは1997年である[7]。近年，病原性*E. histolytica*の中でも有症状者から分離した株と無症状者から分離した株ではその遺伝子型が大きく異なることが報告され，また，*E. moshkovskii*の下痢原性が示唆されるなど，アメーバの種や遺伝子多型にもとづく病原性の違いが改めて注目を集めている[8]。

1．症　状

赤痢アメーバは低酸素状態の大腸粘膜上で細菌に囲まれて生存している。多くの場合は何ら症状を引き起こすことなく，シストの産生・排出を通してそのライフサイクルを維持するが，何らかの原因によってそのバランスが崩れると粘膜に侵入し組織を破壊し病状を引き起こす。赤痢アメーバ症は大腸に病変を生ずる腸アメーバ症と，肝膿瘍などの腸管外アメーバ症とに大別される。シスト摂取から発症までは数日～数カ月かかり，しばしば腹痛，下痢をもって始まる。下痢の頻度は1日に数回～数十回に及び，その血液と粘液の混じった下痢便は本症に特有であり，イチゴゼリー状粘血便とも呼ばれている。

腸アメーバ症の重症度は，病原性，虫体数，宿主の抵抗力によってさまざまで，無症状の者から重症者まできわめて多彩である。軽度の白血球増加や赤沈亢進がみられるが発熱はまれである。下痢と寛解をくり返し慢性化した場合は体重減少や貧血を示す。ときとして劇症型があり，激しい下痢，出血，腸穿孔などを起こして死亡することがあるので注意が必要である。これは，潰瘍性型腸炎と誤診され免疫抑制剤を多用された患者にしばしば認められる。大腸で増殖した栄養型虫体が門脈に入ると肝膿瘍を起こす頻度がもっとも高く，次いで肺，脳，脾臓，肛門周囲の皮膚などに転移する場合がある。もっとも一般的な症状は，右季肋部痛をともなう発熱，肝肥大，悪心，食欲不振などで，右葉に大きく境界鮮明の内部均一な占拠性病変を認める。

2．診　断

診断は臨床症状や所見から当該疾患を疑うことから始まる。その後，①病原体の検出，②病原体のタンパク質やDNAの検出，③補助診断としての病原体に対する抗体検査が行われる。もっとも確実な方法は顕微鏡を用いた下痢便もしくは潰瘍部・膿瘍検体の観察である。偽足を出して活発に動き回る栄養体を認めればアメーバ赤痢である可能性が高い。TechLab社の*E. histolytica* II testを用いたELISA (Enzyme-Linked Immunosorbent Assay) 法による原虫抗原の検出が有効な補助診断となる。

一方，軽症例や無症候例(キャリア)からはシストを検出する頻度が高く，病原性*E. histolytica*と

非病原性 *E. dispar* や *E. moshkovskii* を区別することができない。そのような場合はPCR（ポリメラーゼ連鎖反応）法による赤痢アメーバDNAの検出が有効である[9]。

3．治　療

抗アメーバ剤は肝膿瘍や大腸炎などの組織病変に用いる薬剤（extraintestinal agents）と糞便中への虫体排出を止める薬剤（luminal agents）に大別される。前者にはメトロニダゾール，チニダゾール等のニトロイミダゾール系薬剤（保険適用外）があり，後者にはパロマイシン（熱帯病治療薬研究班保管）等がある。大腸炎や肝膿瘍などの組織内病変に対する第一選択薬はメトロニダゾールである[9]。メトロニダゾールは赤痢アメーバ内のニトロ還元酵素系の反応によって還元を受け，ニトロソ化合物（R-NO）に変化し抗原虫作用を示す。また，反応の途中で生成したヒドロキシラジカルがDNAを切断しDNAらせん構造の不安定化を招く。

本薬剤は赤痢アメーバのみならず，低酸素環境に寄生するランブル鞭毛虫や膣トリコモナス，また，ヘリコバクターピロリなどの偏性嫌気性細菌に対しても有効である。軽症例では750mg/日・分3で5日間投与，腸アメーバ症の重症例やアメーバ性肝膿瘍には1,500mg/日・分3で10日間投与を基本とする。副作用として，しばしば食欲不振，嘔気，味覚異常などが現れる。この場合，減量して様子を見る。末梢神経障害，四肢のしびれ，異常感が認められた場合，投与を中止する。過去に本剤に対する過敏症状を起こした患者，血液疾患患者や妊婦への投与は禁忌である[10]。

4．予防法

飲食物の加熱，手洗いの励行，適切な糞便処理が予防に有効である。発展途上国では人糞に汚染された水による感染が頻繁にみられる。人糞肥料が用いられている場合は農作物を介しての感染の可能性も高い。赤痢アメーバのシストは湿潤な環境では長期間生存しうるが，1分間以上の煮沸により殺滅することが可能であり，また乾燥に弱い。現在のところ，赤痢アメーバに対するワクチンはないが，アメーバの組織定着・細胞接着に重要な役割を果たすgalactose and *N*-acetylgalactosamine（Gal/GalNAc）認識レクチンがワクチン候補分子として有望視されている[11]。

Ⅱ　クリプトスポリジウム症について

クリプトスポリジウム症とは細胞内寄生性原虫クリプトスポリジウム（*Cryptosporidium*）により引き起こされる消化管感染症である。オーシストの経口摂取により感染し（図2），（オーシストは塩素に耐性をもつため）プールや水道水を介して水系伝播する。不顕性感染から嘔吐や発熱などの全身症状をともなう場合まで重症度はさまざまであり，免疫機能が正常な健常人では不顕性感染から1～2週間程度の腹痛をともなう水様性下痢症が認められる。

一方，老人やAIDS患者などの免疫不全状態で

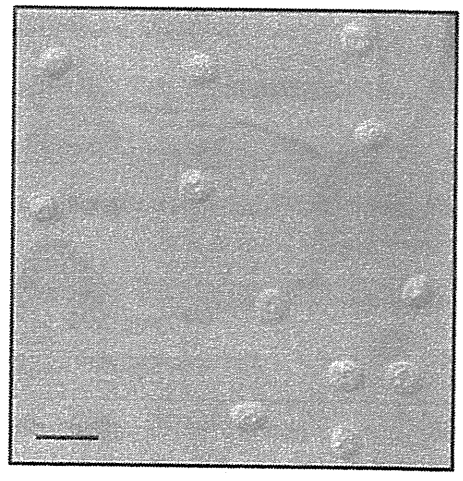

図2　クリプトスポリジウムのオーシスト
クリプトスポリジウムに感染したマウス糞便より精製したオーシスト。オーシストの経口感染によりクリプトスポリジウム症の感染が成立する。微分干渉顕微鏡により撮影した。運動性はない。
（筆者提供）

ELISA（Enzyme-Linked Immunosorbent Assay）
PCR（ポリメラーゼ連鎖反応）
R-NO（ニトロソ化合物）
Gal/GalNAc（galactose and N-acetylgalactosamine）